Millennial-scale climate oscillations triggered by deglacial meltwater discharge in last glacial maximum simulations

Yvan Malo Romé[1], Ruza F Ivanovic[1], Lauren J Gregoire[1], Sam Sherriff-Tadano[1], and Paul Valdes[2]

[1]University of Leeds
[2]School of Geographical Sciences, University of Bristol

November 22, 2022

Abstract

Our limited understanding of millennial-scale variability in the context of the last glacial period can be explained by the lack of a reliable modelling framework to study abrupt climate changes under realistic glacial backgrounds. In this article, we describe a new set of long-run Last Glacial Maximum experiments where such climate shifts were triggered by different snapshots of ice-sheet meltwater derived from the early stages of the last deglaciation. Depending on the location and the magnitude of the forcing, we observe three distinct dynamical regimes and highlight a subtle window of opportunity where the climate can sustain oscillations between cold and warm modes. We identify the European-Arctic and Nordic Seas regions as being most sensitive to meltwater discharge in the context of switching to a cold mode, compared to freshwater fluxes from the Laurentide ice sheets. These cold climates follow a consistent pattern in temperature, sea ice and convection, and are largely independent from freshwater release as a result of effective AMOC collapse. Warm modes, on the other hand, show more complexity in their response to the regional pattern of the meltwater input, and within them, we observe significant differences linked to the reorganisation of deep water formation sites and the subpolar gyre. Broadly, the main characteristics of the oscillations, obtained under full-glacial conditions with realistically low meltwater discharge, are comparable to $\delta^{18}O$ records of the last glacial period, although our simplified experiment design prevents detailed conclusions from being drawn on whether these represent actual Dansgaard-Oeschger events.

Millennial-scale climate oscillations triggered by deglacial meltwater discharge in last glacial maximum simulations

Yvan M. Romé[1], Ruza F. Ivanovic[1], Lauren J. Gregoire[1], Sam Sherriff-Tadano[1], Paul J. Valdes[2]

[1]School of Earth and Environment, University of Leeds, Leeds, UK
[2]School of Geographical Sciences, University of Bristol, Bristol, UK

Corresponding author: Yvan Romé, `eeymr@leeds.ac.uk`

Abstract

Our limited understanding of millennial-scale variability in the context of the last glacial period can be explained by the lack of a reliable modelling framework to study abrupt climate changes under realistic glacial backgrounds. In this article, we describe a new set of long-run Last Glacial Maximum experiments where such climate shifts were triggered by different snapshots of ice-sheet meltwater derived from the early stages of the last deglaciation. Depending on the location and the magnitude of the forcing, we observe three distinct dynamical regimes and highlight a subtle window of opportunity where the climate can sustain oscillations between cold and warm modes. We identify the European-Arctic and Nordic Seas regions as being most sensitive to meltwater discharge in the context of switching to a cold mode, compared to freshwater fluxes from the Laurentide ice sheets. These cold climates follow a consistent pattern in temperature, sea ice and convection, and are largely independent from freshwater release as a result of effective AMOC collapse. Warm modes, on the other hand, show more complexity in their response to the regional pattern of the meltwater input, and within them, we observe significant differences linked to the reorganisation of deep water formation sites and the subpolar gyre. Broadly, the main characteristics of the oscillations, obtained under full-glacial conditions with realistically low meltwater discharge, are comparable to $\delta^{18}O$ records of the last glacial period, although our simplified experiment design prevents detailed conclusions from being drawn on whether these represent actual Dansgaard-Oeschger events.

Plain Language Summary

During the last glacial period (115,000 to 12,000 years before present), the baseline cold climate was continuously disturbed by intense and abrupt climate changes. They completely modified the climate for a few thousand years or so, resulting, for instance, in massive temperature shifts and complete reorganisations of ocean circulation. These abrupt changes have been observed in climate records from the Northern Hemisphere and also can be traced in records from the Southern Hemisphere. Yet, we still do not know what triggers these changes, and often cannot simulate them at the right time under known environmental conditions. In the context of the Last Glacial maximum, a cold period 21,000 years ago with extensive ice over the Northern Hemisphere, this article analyses a new set of climate model simulations that test the effects of freshwater melting from the ice sheets at different periods of the early deglaciation ($\sim$ 21,000 to 18,000 years before present). Under some conditions, the resulting experiments displayed an Atlantic Ocean that oscillates between strong and collapsed basin-wide circulation, causing approximately 10°C of temperature change over Greenland; a behaviour that resembles observed abrupt climate changes.

1 Introduction

The last glacial period was characterised by strong millennial-scale variability (e.g. Bigg & Wadley, 2001; Wolff et al., 2010; Fletcher et al., 2010)., observed through the occurrence of sharp and dramatic shifts in climate state. The best example of such abrupt changes are Dansgaard-Oeschger events (D-O events; Dansgaard et al., 1993). They consist of transitions between cold stadial and warm interstadial climate conditions that occur in cycles as long as six hundred to a few thousand years. Dansgaard-Oeschger events were first identified in $\delta^{18}O$ records of Greenland ice cores (Bond et al., 1993) before also being observed in Antarctica (Blunier & Brook, 2001; Voelker, 2002). Since their discovery, they have been identified in a wide range of different parts of the Earth system, both marine (e.g. Shackleton et al., 2000; Wolff et al., 2010; Dokken et al., 2013; Henry et al., 2016) and terrestrial (e.g. Goñi et al., 2000; Y. J. Wang et al., 2001; X. Wang et al., 2007; Margari et al., 2009; Stockhecke et al., 2016), and can be linked to meridional shifts of the Intertropical Convergence Zone (ITCZ; Peterson & Haug, 2006).

During decades of study, numerous hypotheses have been put forward to understand the underlying mechanisms behind D-O events (a comprehensive list can be found in Li and Born (2019)), and, more generally, millennial scale variability, yet they remain largely unexplained. Nonetheless, at the crossroads of all theories lies the crucial role of the Atlantic Meridional Overturning Circulation (AMOC) (Rahmstorf, 2002; Burckel et al., 2015; Henry et al., 2016). A modification of the thermohaline circulation affects heat and salt redistribution between the tropics and the poles, and consequently has a global-scale impact on the climate (Clark et al., 2002; Rahmstorf, 2002). There is substantial evidence that the AMOC has existed in other configurations (or 'modes') than the one we observe at present times (e.g. Böhm et al., 2015), and that AMOC may thus have the capacity to exist in multiple stable states, as predicted theoretically (Stommel, 1961) and supported by early observations (Broecker et al., 1985) and climate models (Manabe & Stouffer, 1988). Our understanding of abrupt climate change, therefore, relies on uncovering the cause of AMOC mode switches.

The AMOC can be disrupted by freshwater release events in the North Atlantic-Arctic region. They have the power to target vital points of the thermohaline circulation by affecting the ocean density profile at North Atlantic Deep Water (NADW) formation sites (Broecker et al., 1985; Paillard & Labeyriet, 1994; Vidal et al., 1997). In models, freshwater hosing experiments have been widely used to force abrupt climate transitions (e.g. Manabe & Stouffer, 1997; Ganopolski & Rahmstorf, 2001; Kageyama et al., 2010) and observe hysteresis cycles (e.g. Schmittner et al., 2002). They also highlighted the large sensitivity of the climate to the strength and the location of the release, especially in the Greenland, Iceland and Nordic (GIN) Seas (Smith & Gregory, 2009; Roche et al., 2010). Consequently, it is valuable to explore the different sources of freshwater that had the potential to lead to millennial-scale variability.

Iceberg surges during Heinrich events (H events; Heinrich, 1988) recorded by Ice Rafted Debris (IRD) in the North Atlantic (Hemming, 2004), were first candidate to be held responsible for initiating stadial climates. It is now widely accepted that H events are not at the origin of D-O events, they are triggered within stadial states (Barker et al., 2015) and are not recorded at every D-O occurrence (Lynch-Stieglitz, 2017). Instead, we can conceive of them as a likely response to the earlier climate-ocean perturbation or even a positive feedback mechanism for perpetuating/amplifying stadial climates (Ivanovic et al., 2018). Meltwater released from the long term deglaciation of ice sheets was another significant source of freshwater during the last glacial period (Gregoire et al., 2012), although only a few studies have investigated the influence of such 'background' melt (e.g. Ivanovic et al., 2018; Kapsch et al., 2022; Matero et al., 2017), probably because it requires precise constraints on the ice sheet geometry and history of melt/growth (Bethke et al., 2012). Holding the most complete records of ice sheet evolution, both in terms of spatial and temporal resolution, (e.g. Dyke, 2004; Hughes et al., 2016; Briggs et al., 2014; Bradwell et al., 2021), the last deglaciation (and especially its early phase, $\sim$ 21–16 ka BP, thousand years before present) offers the perfect setting to assess the ability of the early phase of continental deglaciation (i.e. the long-term background melt from disintegrating ice sheets) to generate millennial-scale variability in glacial conditions.

The last deglaciation initiated from the Last Glacial Maximum (LGM; $\sim$ 21 ka, (Clark et al., 2009), which corresponds to a maximum in continental ice sheet extent in the Northern Hemisphere (Batchelor et al., 2019) shaped during the preceding glacial period. The upper cell of the AMOC was likely shallower, but it is not known whether it was stronger or weaker than present day (Gebbie, 2014; Lynch-Stieglitz, 2017; Muglia & Schmittner, 2021). A steady increase in Northern Hemisphere summer insolation (Berger, 1978) triggered the long-term demise of the Laurentide and Eurasian ice sheets, with rising concentrations of atmospheric CO_2 positively reinforcing the deglaciation (Gregoire et al., 2015). However, while Southern Hemisphere temperatures gradually rose (Parrenin et al., 2007), the climate in the North remained cold for several thousand years; a period known as Heinrich Stadial 1 (∼18–15 ka BP) (Denton et al., 2006; Roche et al., 2011; Ng et al., 2018). The most recent of Heinrich events, H1 (Hemming, 2004; Stanford et al., 2011), began some two thousand years after the onset of Henirich Stadial 1 (Stern & Lisiecki, 2013; Hodell et al., 2017). In the years of deglaciation that followed the LGM, several millennial scale events were observed (Weber et al., 2014). Two episodes are particularly relevant to our study: the sudden Bølling Warming (∼ 14.5–13 ka BP; Severinghaus & Brook, 1999) concurrent with an intensification of the AMOC (Ng et al., 2018; Du et al., 2020), and the ensuing Younger Dryas, when Northern Hemisphere climate abruptly returned to a stadial state with glacial re-advance (∼ 13–12 ka; Murton et al., 2010; Liu et al., 2012). While not formally identified as D-O events, similarities in climate and ocean evolution between these last deglaciation and D-O oscillations have prompted others to at least draw analogies between them, and to speculate on whether they have a common cause (e.g. Obase & Abe-Ouchi, 2019).

Simulating climate oscillations in glacial conditions has proven to be very challenging, and even more so during the LGM. This is because of the strong feedback between the large ice sheets and wind stress, deep water formation and energy balance (Oka et al., 2012; Ullman et al., 2014; Beghin et al., 2015; Roberts & Valdes, 2017), which act to intensify, or at least stabilise, the AMOC (Oka et al., 2012; Klockmann et al., 2016; Sherriff-Tadano et al., 2018). Most models from both the Paleoclimate Modelling Intercomparison Project Phase 3 (PMIP3; Muglia & Schmittner, 2015) and Phase 4 (PMIP4; Kageyama et al., 2021) tend to simulate a deeper and stronger NADW than inferred from palaeo records, which could explain why few modelling studies have observed millennial scale variability in glacial background (e.g. Klockmann et al., 2018). In order to trigger abrupt climate transitions, freshwater hosing experiments have historically needed to overestimate fluxes as reviewed by Kageyama et al. (2010) (e.g. Liu et al., 2009; Menviel et al., 2011), and have not succeeded in simulating abrupt changes when using 'realistic' fluxes (Bethke et al., 2012; Gregoire et al., 2012; Snoll et al., 2022). Obase and Abe-Ouchi (2019) have arguably come the closest to overcoming this meltwater 'paradox' by simulating the Bølling Warming even with some deglacial meltwater forcing. However, even they require a significantly lower than likely freshwater discharge from the deglaciating ice sheets (e.g. Peltier et al., 2015).

The dispute over what could feasibly cause abrupt climate changes not directly driven by freshwater fluxes led the community to start actively searching for oscillating behaviours in their models. At the same time, the criticism that simulations integrated for only a few hundred or a thousand years should not be considered to have a steady-state or 'spun-up' ocean circulation began to gain traction (Marzocchi & Jansen, 2017; Dentith et al., 2019), prompting modellers to run long simulations with higher-order climate models — made possible by the increase of computational power — in order to examine long-term drifts. It is therefore probably not a coincidence that more and more coupled Atmosphere-Ocean General Circulation Models (AOGCMs) have reported observing AMOC mode oscillations in recent years (e.g. Peltier & Vettoretti, 2014; Brown & Galbraith, 2016; Klockmann et al., 2018; Sherriff-Tadano & Abe-Ouchi, 2020). They have been achieved under a range of different freshwater hosing scenarios (e.g. Cheng et al., 2011), atmospheric CO_2 concentrations (e.g. Zhang et al., 2017) and ice sheet geometries (e.g. Klockmann et al., 2018), although, to our knowledge, only Peltier and Vettoretti (2014) managed to obtain AMOC oscillations under glacial maximum conditions.

To sum-up the combined results from these studies, there seems to exist a window of opportunity (Barker & Knorr, 2021) in each model's inputs (parameter values, boundary conditions and forcings) and background climates where oscillations can establish and sustain (e.g. Peltier & Vettoretti, 2014; Brown & Galbraith, 2016; Klockmann et al., 2018). The ice sheets' layout in particular has a strong influence on the local and global climate, including on the atmospheric circulation (Löfverström et al., 2014; Roberts et al., 2014; Sherriff-Tadano et al., 2021), the gyres (Gregoire et al., 2018), the energy balance (Roberts & Valdes, 2017) and freshwater fluxes (Matero et al., 2017). As a result, the new generation of better constrained and more detailed ice sheet reconstructions such as ICE-6G_C (Peltier et al., 2015; Argus et al., 2014) and GLAC-1D (Tarasov & Peltier, 2002; Tarasov et al., 2012; Briggs et al., 2014; Ivanovic et al., 2016) may prove to be decisive in whether or not the 'right' conditions for triggering abrupt climate changes are obtained.

In this paper, we present our contribution to this initiative in the form of a new set of LGM simulations forced with deglacial meltwater. Inspired by an initial experiment that showed millennial-scale variability under a transient meltwater forcing, we designed our simulations with fixed meltwater inputs in order to be able to describe the oscillations in detail and evaluate the sensitivity of the oscillatory behaviour to meltwater patterns. These inputs were derived from snapshots of the early deglaciation meltwater history (specifically, between 21.5 and 17 ka BP) calculated from GLAC-1D ice sheet reconstruction.

Depending on the freshwater pattern, we observe three different dynamical regimes, including regular and self-sustained climate oscillations. The oscillations are characterised by switches between strong, shallow glacial AMOC and near- or completely- collapsed AMOC modes, a Greenland surface cooling/warming of $\sim 10°$C, and a periodicity of about 1,500 ka. This regime can be sustained for about 10,000 years (the maximum length of the experiments). These are, to our knowledge, the first general circulation model simulations to use ice sheet reconstruction-derived distributions of meltwater to produce strong AMOC oscillations under glacial maximum climate conditions, and to investigate the sensitivity of the oscillations to patterns of meltwater discharged to the ocean.

The non-oscillating clusters of our experiments inform us of the pre-requisite conditions for passing through the oscillating window. Here, we describe the various simulations in detail, their oscillatory or non-oscillatory climate/ocean states, and the different Earth system components involved in the abrupt events. We conclude with a discussion on the relevance of our simulations in the context of known past abrupt climate changes. The design introduced in this study allows us to undertake a relatively systematic set of sensitivity tests of the impact of realistic freshwater distributions (albeit for unrealistic lengths of time) on ocean circulation, with the multi-millennial integrations enabling us to explore the long-term effect of each pattern.

2 Methods

2.1 The model

The simulations introduced in this article were completed using the BRIDGE (Bristol Research Initiative for the Dynamic Global Environment group) version of the HadCM3 atmosphere-ocean general circulation model (GCM) (Valdes et al., 2017). This GCM consists of a 19 layers $\times$ 2.5° $\times$ 3.75° atmosphere model more completely described by Pope et al. (2000), coupled every simulation day with a 20 layers (up to 5,500m deep) $\times$ 1.25° $\times$ 1.25° ocean model, described by Gordon et al. (2000) (Bryan & Cox, 1972; Fofonoff & Millard Jr, 1983; Fofonoff, 1985). This version of HadCM3 includes the MOSES 2.1 land model (P. M. Cox et al., 1999), and the TRIFFID dynamic vegetation model (P. Cox, 2001). HadCM3 has been tested in many different scenarios (I.P.C.C., 2014; Reichler & Kim, 2008), and was optimised for running multi-millennial simulations (Valdes et al., 2017).

2.2 Experimental design

The LGM simulation that makes up the base climate state for all simulations presented here was created following the PMIP4 protocol for 21 ka BP (Kageyama et al.,

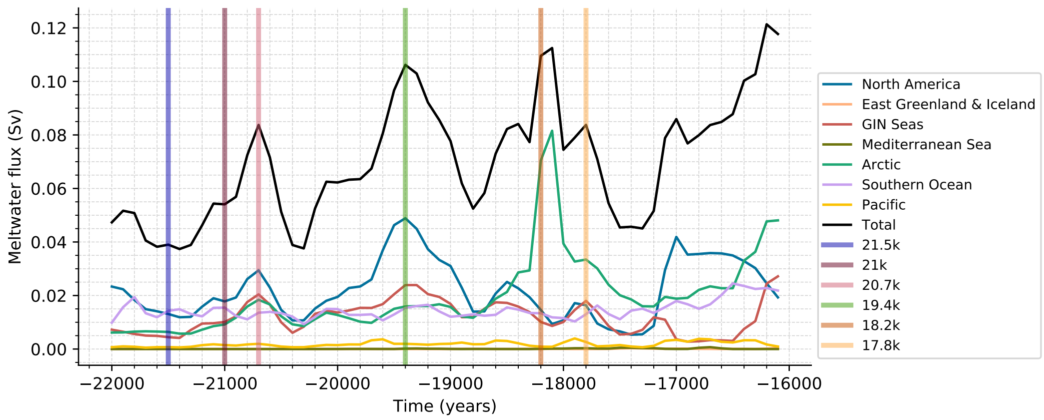

Figure 1. Meltwater discharge history over the early deglaciation and its distribution over key regions (defined in Figure S2*b*). This plot incorporates the 200-years smoothing described in section S2. Vertical bars represent the time steps chosen for calculating each constant meltwater-forcing snapshot (see section 2.2, and Table 1).

2017) using the GLAC-1D ice sheet reconstruction (Tarasov & Peltier, 2002; Tarasov et al., 2012; Briggs et al., 2014; Ivanovic et al., 2016); see section S1 (Bereiter et al., 2015; Loulergue et al., 2008; Schilt et al., 2010). This new HadCM3 LGM simulation was initialised from a chain of existing multi-millennial HadCM3 PMIP3 LGM simulations, which were started from multi-millennial continuations of earlier HadCM3 LGM simulations (Davies-Barnard et al., 2017), giving a pre-PMIP4 LGM spin-up of several thousand years. The new PMIP4 GLAC-1D set-up was integrated for 3,500 years, and the end of this final spin-up phase provides the initial condition for all simulations presented here. We continued the LGM simulation for a further 4,000 years in parallel with our other experiments to provide a reference climate state (*CTRL*) for comparison to the other simulations. There are small, steady drifts in the ocean over the run (Figure S5), but the signal of the trends are dwarfed in comparison to the changes of interest described below, and little is gained for this study by extending *CTRL* further. The starting year of *CTRL* is defined as year 0.

GLAC-1D has rarely been used for LGM simulations compared to the other ice sheet reconstructions (Kageyama et al., 2021) such as ICE-6G_C (Peltier et al., 2015) and the PMIP3 ice sheet (Abe-Ouchi et al., 2015). It was preferred for this study because compared to the alternative reconstructions, it includes more recent constraints on the Eurasian ice sheets (provided by the DATED-1 project; (Hughes et al., 2016), a region that could be crucial for accurately capturing the early deglacial climate history (Ivanovic et al., 2018). A transient meltwater history was derived from GLAC-1D's representation of the deglaciation (section S2). We decided against using the transient meltwater flux, because the added complexity introduced by the temporal variability and possible ocean 'memory' of the preceding [uncertain] meltwater history would have convoluted the physical interpretation of our results. Instead, we examined the triggering of abrupt climate changes using a simpler approach; by selecting six interesting, different, fixed-forcing scenarios (our 'snapshots'), that allow us to investigate the sensitivity of the glacial ocean and surface climate to early deglacial freshwater inputs (Figure 1).

The snapshots were identified for their ability to collectively capture a broad range of possible situations that may have led to changes in ocean circulation and surface climate. The six scenarios correspond to different modes of discharge and are named after the period they were extracted from (see Figure 1); see Figure S2*c* for the spatial dis-

Simulation	Meltwater (Total flux)	Integration length	Category	Salinity Target (PSU)
CTRL	None	4,000 years	reference	35.8334
21.5k	21.5 ka (0.039 Sv)	4,000 years	warm	35.834
21k	21 ka (0.054 Sv)	4,000 years	warm	35.8334
20.7k	20.7 ka (0.084 Sv)	10,000 years	oscillating	35.8225
19.4k	19.4 ka (0.106 Sv)	10,000 years	oscillating	35.7901
18.2k	18.2 ka (0.109 Sv)	10,000 years	slow-recovery	35.7348
17.8k	17.8 ka (0.084 Sv)	10,000 years	oscillating	35.7125

Table 1. Experiments summary. All experiments were designed with LGM boundary conditions, using the LGM GLAC-1D ice sheet extent and associated geographies. Entries in the *Category* and global mean *Salinity Target (PSU)* columns are explained in sections 4 and 2.2, respectively.

tribution of the fluxes. The *21.5k*, *21k* and *20.7k* snapshots were chosen for being close to the LGM, sharing a similar distribution, but with different rates of meltwater discharge. The *19.4k* snapshot hosts a strong Labrador Sea/North Eastern American coast/Gulf of Mexico discharge (shortened to 'North American' discharge hereafter), but has a relatively small meltwater flux to the Arctic. Conversely, *18.2k* and *17.8k* have high Arctic and low North Atlantic discharge, with *18.2k* having the most freshwater entering the Arctic. These six snapshots of the deglacial meltwater history were used as forcing for six new equilibrium-type (i.e. constant-forcing) simulations, started from year 0. The meltwater inputs were kept constant throughout the runs.

Table 1 presents a summary of all experiments. The difference between any of them is the prescribed ice sheet meltwater (or absence of it, in *CTRL*).

The idea of having a continuous fixed meltwater discharge for thousands of years is unrealistic by nature. However, in the most extreme scenario (*18.2k*), the total forcing corresponds to a sea level rise of 102 m in 10,000 years, which, for context, is still less than what has been reconstructed for the whole of the last deglaciation (Lambeck et al., 2014). It therefore remains appropriate to consider our results in light of glacial and deglacial variability in order to understand the effect of the forcing, though we are careful to highlight that this is not a transient simulation of deglacial meltwater. To avoid long-term drifts in mean ocean salinity caused by the long freshwater forcing, we impose a constant global mean salinity target (following the *VFLUX* method of Dentith et al. (2019) commensurate with the starting condition for each 'snapshot' (Table 1). The salinity target conserves water in relation to terrestrial ice volume (applied as relative to the present day) and thus, in the context of these simulations, counteracts global freshening by removing the excess water as a very small proportion of freshwater from every ocean grid cell at every ocean model timestep (one hour). This approach is in keeping with the snapshot/equilibrium experimental design whilst still allowing the ocean to 'feel' the surface forcing. See section S3 for details.

Most simulations were run for 10,000 years; long enough to characterise their climate behaviours. However, like *CTRL*, two simulations (*21.5k* and *20.7k*), were terminated after 4,000 years. At this point, little was changing in those simulations, and since no further time series were required for the analysis, we opted to conserve the computing resource.

Some simulations experienced numerical instability in the stream function off the coast of the Philippines after a few thousand years. This quirk was resolved by smoothing the bathymetry in the region of the instability and restarting the run a few years before the instability arose. More information, including the detail of the smoothing algorithm and its very minor impact on the climate response, is given in section S4.

2.3 Characterising oscillations and defining warm/cold-mode composites

All experiments apart from *CTRL* show some kind of alternation between weaker and stronger AMOC phases, or 'modes'. Changes in the AMOC are correlated to increases and decreases in NGRIP temperatures (North Greenland Ice Core Project, 42.32° W, 75.01° N) and so we will also refer to these phases as 'cold' and 'warm' modes, respectively. We do not use the terms *stadial* and *interstadial* to describe the cold and warm states because of the complicated connotations associated with these terms, but they may be thought of in such a light.

In order to characterise oscillations in the simulations, we applied a filtering algorithm and Fourier analysis to derive the spectrum of the temperature time series at the location of NGRIP, see section S5 for details. If there is a peak in the spectrum, then oscillations can be defined and described, and we we apply a Butterworth low-pass filter to screen-out the frequencies lower than the millennial-scale variability of interest.

We also found it useful, in our analysis, to examine characteristics common to all warm and cold modes in the suite of simulations. Thus, to build a composite of the two modes from the time series of results, we defined quantitative boundaries bespoke to each simulation (it proved ineffective to adopt a consistent definition for all simulations because of their differences). Points below the weak limits (in AMOC strength/NGRIP temperature) were added to the composite cold mode and points above the strong limits were added to the warm modes. This approach is described in section S6, where we demonstrate that the choice of how to define the composite modes does not significantly impact the results, and that to manually set up the weak and strong limits was an easy and robust method to build the composite states.

3 A new weak, shallow AMOC LGM simulation

The *CTRL* run replicates and continues the HadCM3-GLAC-1D LGM simulation presented in Kageyama et al. (2021). The global mean surface temperature is 6.6°C colder than Pre-Industrial (PI). Compared to other PMIP4 simulations, this simulation is in the coolest range, almost 2°C below the average mean temperature, and is colder than any PMIP3 simulations analysed by Kageyama et al. (2021), yet close to the current estimate from global temperature reconstructions ($\sim 6.1°C \pm 0.4°C$ cooler than PI in Tierney et al. (2020), $\sim 7.0 \pm 1.0°C$ cooler than PI in Osman et al. (2021). The global mean ocean surface temperature cools by 3.4°C, which is significantly cooler than the $\sim 1.7 \pm 0.1°C$ cooler than PI inferred by Paul et al. (2021), but again is a good match to the reconstruction by Tierney et al. (2020) ($\sim 3.1 \pm 0.3°C$ cooler than PI). Contrary to most PMIP4 models, HadCM3 produces an AMOC that is both shallower and weaker in a full-glacial background compared to its pre-industrial state, although AMOC is still vigorous with a maximum strength of 20 Sv at 30° N. We also note that the simulation gets slightly cooler when using GLAC-1D compared to ICE-6G_C (Ivanovic et al., 2018), despite similar values for the maximum overturning circulation.

A summary of the *CTRL* equilibrium climate is shown by Figure 2. The thermohaline circulation is fuelled by intense convection in the northeast Atlantic, with deep water formation sites located primarily south of Iceland and west of the British Isles (Figure 2*b*). This creates a corridor in the eastern part of the Atlantic where warm waters can transit to high latitudes, while the western part of the ocean gets covered by winter sea ice and observes a much cooler climate (Figure 2*c*). The winter sea ice layer extends towards the East of the North Atlantic basin, creating a strong North-South gra-

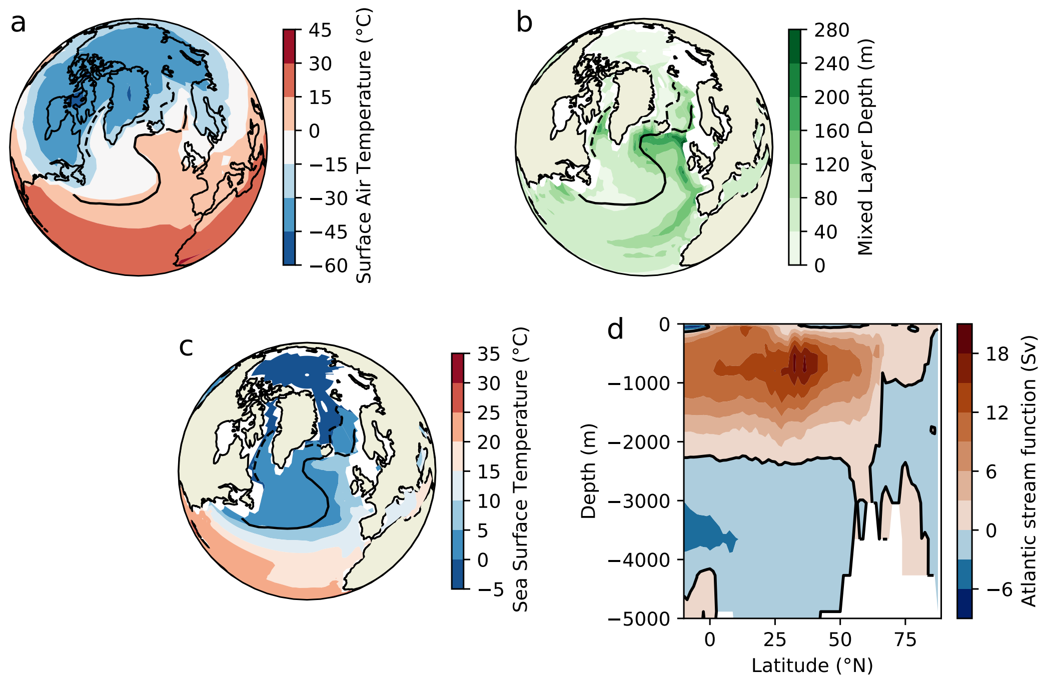

Figure 2. Mean annual conditions between simulation years 3900 and 4000 for *CTRL*. *a.* Surface air temperature. *b.* Mixed layer depth. *c.* Sea surface temperature. *d.* Meridional overturning stream function in the Atlantic basin. Dashed/solid lines indicate the March/September 50% sea-ice extent.

dient in atmospheric temperature in this region (Figure 2*a*). The Arctic Ocean is covered in sea ice all year long. Dense waters sink in the Labrador Sea when the sea ice is less extensive in this region in late autumn.

4 Climate response to the meltwater perturbations

We observe significant differences in the climate response of the six meltwater experiments (Figure 3), best encapsulated by the evolution of the AMOC index. For this study, we define the AMOC index as the maximal value of the overturning circulation in the Atlantic ocean at 26.5° N. This index corresponds to the modern RAPID-array AMOC measurement grid (Smeed et al., 2014) and has been regularly used in palaeostudies (e.g. Guo et al., 2019).

The meltwater simulations can be assigned to three different regimes, or clusters, according to the AMOC index (Figure 3*b*). In the first grouping, simulations *21.5k* and *21k* returned to the reference state after a short cooling event during the initial years of the forcing, when the ocean adjusts to the introduction of the weak meltwater fluxes. This AMOC decline lasted for approximately 500 years, with the index weakening by as much as 5 Sv for *21k* and 1.5 Sv for *21.5k* approximately halfway through this initial cooling. While *21.5k* hardly recorded a change of polar temperatures (Figure 3*c*), the drop in *21k* AMOC strength drives up to 5°C cooling over Greenland. Neither simulation shows a strong response over Antarctica (Figure 3*d*). Accordingly, *21.5k* and *21k* will be referred to as *warm simulations* (note that with an LGM baseline climate, this term is relative).

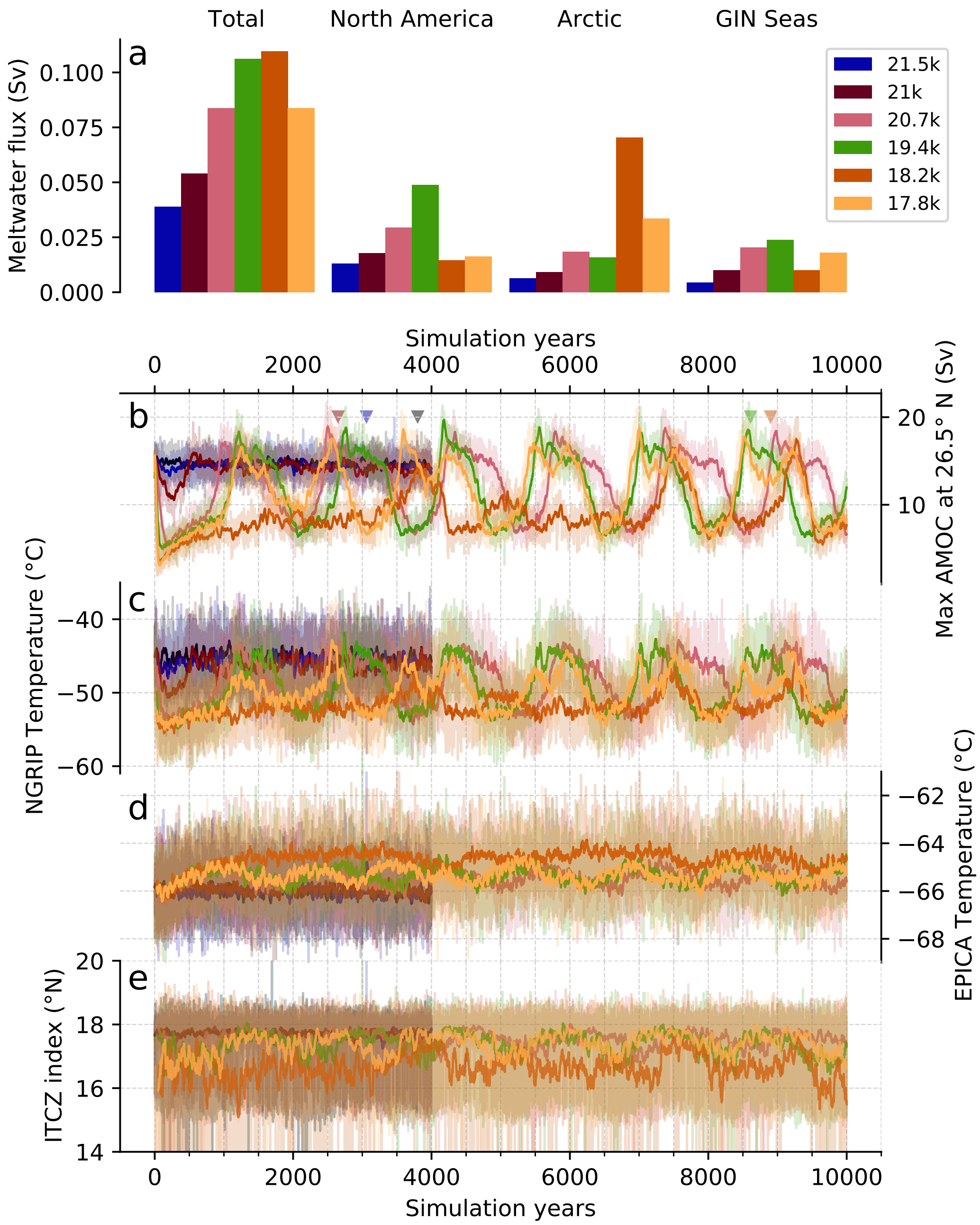

Figure 3. *a.* Snapshot experiments' total meltwater discharge and distributions, summarised (the three main regions are defined in Figure S2. *b.* AMOC index (max Atlantic overturning circulation at 26.5° N). *c.* Greenland Surface Air Temperatures at NGRIP (42.32° W, 75.01° N). *d.* Antarctica Surface Air Temperatures at EPICA Dome C (Concordia Station of the European Project for Ice Coring in Antarctica, 123.21° E, 75.06° S). *e.* Intertropical Conversion Zone index (corresponding to the simulated mean Northern extent of the equatorial rain belt, defined in section S7, inspired by Braconnot et al. (2007) and Singarayer et al. (2017)). Solid lines represent the 30-years running mean and transparent envelopes represent inter-annual variability, except for panel *e*, where the solid line is the 50-year running mean for ease of readability. Arrows indicate the date of the application of localised bathymetric-smoothing (see section S4) for *21k*, *21.5k* and *CTRL* (left to right).

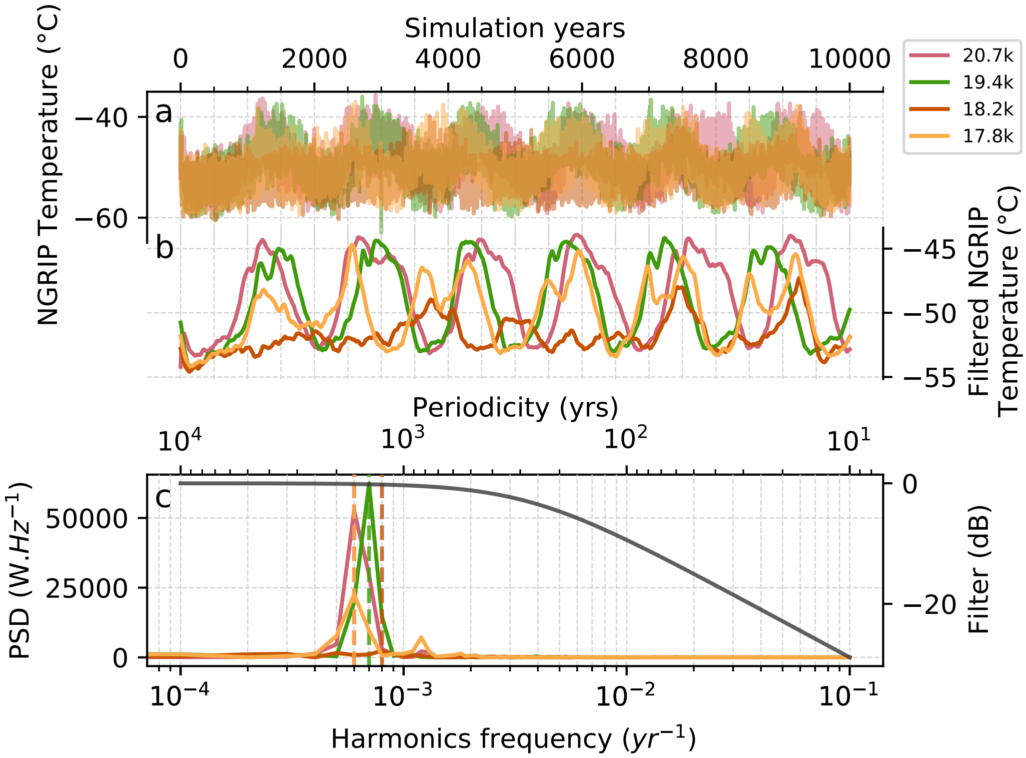

Figure 4. Spectral analysis of simulated surface air temperature through time above NGRIP (42.32° W, 75.01° N). *a.* Unfiltered signal for *oscillating* and *slow-recovery* simulations. *b.* Filtered response, using first class low-pass Butterworth filter. *c.* Power Spectral density (PSD, left hand scale) of the unfiltered signal. Dotted lines indicate the dominant frequency/period for each simulation. Grey line in panel *c* shows the bode diagram of the low-pass filter. Simulations *21.5k* and *21k* are not shown as their Fourier analysis was not conclusive.

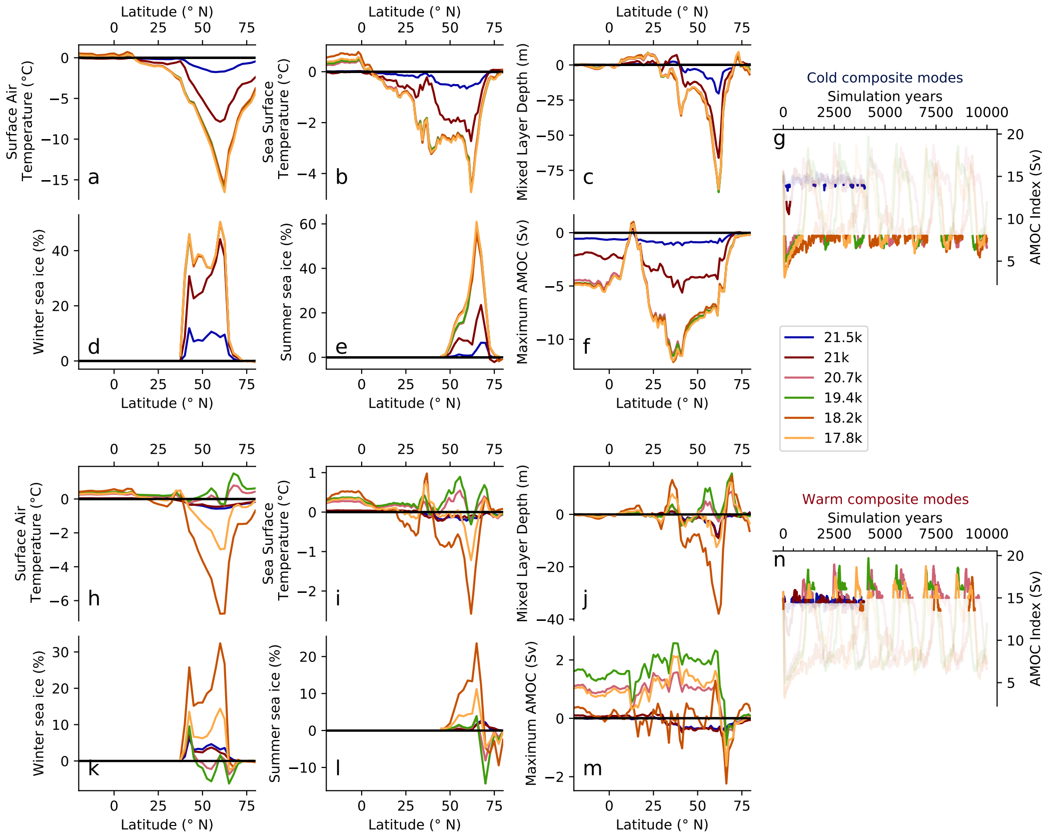

Figure 5. Composite cold and warm modes' mean zonal anomalies between the meltwater simulations and the reference state in the Atlantic (70° W – 10° E). For cold modes (top), panels show the zonally averaged *a.* surface air temperature, *b.* sea surface temperature, *c.* mixed layer depth, *d.* winter sea ice concentration, *e.* summer sea ice and *f.* maximum overturning circulation flow over the water column. For warm modes (bottom), panels show the zonally averaged *h.* surface air temperature, *i.* sea surface temperature, *j.* mixed layer depth, *k.* winter sea ice concentration, *l.* summer sea ice and *m.* maximum overturning circulation flow over the water column. For orientation, an AMOC time series highlighting the periods contributing to the composite cold and warm modes is shown by panels *g* and *n*, respectively.

In a second regime of its own, the AMOC in *18.2k* almost entirely collapsed as soon as meltwater was discharged, causing Northern Hemisphere cooling and a significant shift southward of the ITCZ (Figure 3*e*). Short recovery episodes occur at irregular intervals through the 10,000 years of the simulation, but they cannot be sustained for longer than a few hundred years. This simulation will be labelled a *slow-recovery simulation*.

Finally, through Fourier analysis (Figure 4*c*; section 2.3) we identify three *oscillating simulations* (*20.7k*, *19.4k* and *17.8k*). They switch to a cold state at the onset of the run and continue in a quasi-oscillating regime between cold (near collapsed AMOC, similar to *18.2k*) and warm modes (equivalent or stronger AMOC with respect to *CTRL*). The three *oscillating simulations* behave in a similar way and will be described in more detail in the following sections.

During the cold modes (Figure 5, top), we observe strong consistency between the *oscillating simulations* and the *slow-recovery simulation*, to the point where it becomes almost impossible to distinguish between them. These experiments show a maximum in atmospheric and oceanic cooling around 60° N (Figure 5*a*, *b*), where sea ice cover is now present both in winter and summer after the deep water formation sites vanished (Figure 5*c*–*e*). A second peak of winter sea ice is noticeable around 40° N, but is not as clear in summer sea ice nor mixed layer depth. This second peak corresponds to the closing of the warm water corridor off the western coast of Europe and the spread of winter sea ice in this region. It is around these latitudes that we observe a maximal reduction of the thermohaline circulation by up to 14 Sv (Figure 5*f*). Because of the loss of convection at high latitudes, the upper cell of the AMOC largely dwindles north and south of 20° N. The *warm simulations* follow a similar pattern of disruption, but are not nearly so intense. In *21.5k*, the soft decline of the AMOC is consistent with a shift southward of the convection sites, most likely resulting from a slightly cooler North Atlantic climate (Figure 5*c*–*f*). Summer sea ice extent is very similar to *CTRL* values in *21.5k*. The slowdown of the AMOC is slightly more pronounced in *21k*, with a clear reduction of sea surface temperature by as much as 2°C and of surface air temperature by up to 7.5°C at high latitudes (Figure 5*a*, *b* and *f*). It is remarkable that *21k*'s winter sea ice expansion and mixed layer depth shallowing are comparable to the *oscillating* and *slow-recovery* simulations, demonstrating an increased seasonality compared to the reference *CTRL* state (Figure 5*c*–*d*).

We do not observe such consistency between simulations during their warm modes (Figure 5, bottom). They all show a significant recovery from the cold modes, but it is impossible to underline a single common behaviour. For example, despite a couple of periodic recovery phases of the AMOC in *18.2k* (around 3,500, 7,000 and 9,000 years into the run; Figure 3*b*), the warm modes remain in a relatively cold-climate state (Figure 5 *h*–*i*). At 60° N, sea surface temperatures are down 2°C and surface air temperatures drop by 6.5°C compared to *CTRL*. Shallower mixed layer depths around the same latitude indicate that Iceland/Irminger Basin and Labrador Sea convection sites are still greatly disrupted (Figure 5*j*). This keeps the sea ice edge far south in both summer and winter (Figure 5*k*–*l*). On the other hand, the strong modes of the *warm simulations* are comparable to the reference *CTRL* state, only with a slightly cooler climate (Figure 5*i*–*j*) and a slower overturning circulation above 30° N in the Atlantic (Figure 5*m*). Amongst the *oscillating simulations*, the AMOC index is stronger than in *CTRL* (Figure 5*m*), increasing by as much as 2 Sv in the subpolar region. However, for the most part, these simulations also show disparities in key climate descriptors, at least in terms of amplitude of the anomalies. Surface temperatures and sea ice extent in *18.2k* and *17.8k* bear the closest resemblance across this subset of simulations, whereas temperatures and sea ice extent in *20.7k* and *19.4k* indicate a slightly warmer climate (Figure 5*h*, *i*, *j*, *l*) despite there being stronger ocean convection in *17.8k* (Figure 5*j*). The oscillating simulations all show an increase in winter sea ice around 40° N compared to *CTRL*, corresponding to the narrowing of the warm water corridor along the coast of western Europe (Figure 5*k*). In summary, none of the simulations exactly returned to the *CTRL* reference climate during their respective warm modes, indicating significant regional legacy induced by the imposed meltwater patterns.

5 Influence of the meltwater discharge

Abrupt climate changes are triggered by constant meltwater discharge in our simulations. Yet, we observe a strong non-linearity between the climate response and the location and the influx of freshwater, (Figure 3). For instance, despite a similar total influx of about 0.1 Sv, *19.4k* is tipped into an *oscillating* regime while *18.2k* ends up in a *slow-recovery* state. On the other hand, *20.7k* and *19.4k* display similar oscillating dynamics even though the total flux is around 20% weaker in *20.7k* than *19.4k*. All of this hints at the importance of differences in the meltwater discharge pattern. However, whilst the spatial distribution of freshwater forcing is comparable between *21k* and *20.7k*, only

20.7k manages to generate oscillations, demonstrating that while the spatial distribution of the freshwater flux is an important control on the oceanic response, there is also a sweet spot in the perturbation conditions where the forcing needs to be strong enough to trigger a switch to stadial states, but not so strong that it (semi-)permanently suppresses a recovery as in *18.2k*.

A threshold is reached in the cold climate modes, when the climate cools so far that it becomes insensitive to further meltwater discharge (Figure 5). Independent of the forcing, all simulations produce a similar spatial pattern in temperature, sea ice and deep water formation layout during the weak phases, but only when the surface atmosphere cools by as much as 15°C does the climate cross a tipping point where the cold phases can be sustained for a few hundred years. This corresponds to the vanishing of all oceanic convection north of 40° N (Figure 5*c*), resulting in an almost collapsed AMOC (up to 12 Sv weaker) in the North Atlantic (Figure 5*f*). When all the deep water formation sites have vanished, the response becomes decoupled from the forcing and only smaller regional effects can be induced. This phenomenon resonates with the conclusion of Smith and Gregory (2009).

During warm AMOC modes, the differences in climate response seem to be driven by the regional patterns of discharge. The influence of the different forcings can be tracked by creating a composite of warm modes mixed layer depth anomalies (Figure S10), producing clearly distinct results from the *warm* simulations, the simulations with prevalent North American meltwater inputs (*20.7k*, *19.4k*) and the simulations dominated by Arctic discharge (*18.2k*, *17.8k*). However, this relationship is sometimes counter-intuitive. For instance, despite having a stronger North American forcing in *19.4K* than in *18.2k* and *17.8k*, Labrador sea deep water formation is more impacted in the latter two simulations. In addition, although *18.2k* and *17.8k* have high Arctic discharge, Iceland Sea convection intensifies and the Irminger Basin convection weakens.

The effect of Arctic/GIN Seas discharge is decisive for triggering the shift from warm to cold AMOC states and leads to the strongest modification of the warm modes (Figure 5). The two most disrupted warm stages are found in *18.2k* and *17.8k*, both dominated by Arctic discharge. We infer that this comes from the relative position of other convection sites. For example, when released in the Arctic, freshwater follows the Greenland currents to reach the Irminger/Iceland basins relatively quickly, thus having undergone less dispersal than if taking a longer more circuitous route, particularly compared to meltwater entrained in the Atlantic gyres (Born & Levermann, 2010). Arctic meltwater will thus target the main deep water formation sites without having been significantly mixed into becoming warmer and saltier waters. Meltwater entering the GIN Seas should play a similar role, but the relatively low discharge in this area in our simulations makes it hard to conclude with certainty, and could explain why we do not observe a strong signal in this region (Figure S10).

Meltwater released off the northeast coast of North America have a weaker impact. Simulation *19.4k* has greater North Atlantic discharge, and similar fluxes to the Arctic and GIN Seas compared to *20.7k*. However, this increase in North Atlantic meltwater does not drive any significant ocean or climate response. Here, again, the explanation may relate to the location of the deep water formation sites. Because Labrador Sea convection is not always active, and easily shut down in our simulations, freshwater has to transit all around the subpolar gyre to target the more crucial sites in the eastern North Atlantic. By then, it has been mixed with tropical waters, weakening the forcing. The increased sensitivity to Arctic discharge compared to North American discharge in our simulations ties in with the conclusions of Roche et al. (2010) and Condron and Winsor (2012).

The existence of a sweet spot in the rate and location of meltwater discharge to the ocean for triggering climate transitions also depends on the background climate. Understanding the conditions leading to the creation of such a window of opportunity (Barker & Knorr, 2021) where abrupt climate changes can arise has been widely discussed (e.g. Brown & Galbraith, 2016; Zhang et al., 2017; Klockmann et al., 2018). Among the parameters likely to influence it, the choice of ice sheet reconstruction seems key, even more so in our simulations, as we rely on it both for the background climate state and for the meltwater forcing scenarios. In previous HadCM3-family deglaciation studies (e.g. Ivanovic et al., 2018; Gregoire et al., 2012), different ice sheets reconstructions did not yield as significant climate transitions, in spite of having a comparable baseline climate state (Kageyama et al., 2021) and magnitude of forcing. The higher temporal resolution of GLAC-1D and its treatment of the Eurasian ice sheet makes it a perfect candidate to attain this subtle balance, as hypothesised by Ivanovic et al. (2018). Precisely what about this particular reference state provides such a compliant framework for simulating AMOC oscillations may form the basis of future study, but we can reasonably hypothesise that very high-latitude meltwater is a pre-requisite for obtaining the sweet spot for producing climate variability, since without it, no oscillations are observed.

6 Bimodal warm states linked to reorganisation of deep water formation and subpolar gyre layout

Intriguingly, the *oscillating simulations* frequently undergo a double warm peak during times of strong AMOC (Figure 4*b*). This is particularly clear in the late cycles of *17.8k* (i.e. after 3,000 years), where the first peak in each warm phase is slightly cooler than the second. It indicates two distinct climate states separated by a cooling and then warming transition that is lower in amplitude than the cold-AMOC to warm-AMOC mode shift and which do not resemble the classical two-stage recovery hypothesis described by Renold et al. (2010) and Cheng et al. (2011). Changes in sites of deep water formation and the SubPolar Gyre (SPG) have been at the centre of recent studies of abrupt climate and ocean circulation changes (Li & Born, 2019; Klockmann et al., 2020) and could shed some light on this warm-mode transition stage. Hence, we next examine the relationship between the AMOC index, the longitude of the centre of Mass of the Mixed Layer Depth (MLD COM) and different physical indicators.

There is a linear relationship of roughly $1^{\circ}\mathrm{C\,Sv^{-1}}$ between the AMOC index and the temperature at NGRIP (Figure 6*a*), demonstrating once again that AMOC index and NGRIP temperatures are interchangeable when it comes to identifying climate modes in our simulations. The intensity of the convection sites follow a similar trend (Figure 6*b*), with roughly a 10 metre increase of the maximum mixed layer depth in the North Atlantic for each degree of warming over Greenland. Both these relationships remain consistent irrespective of the specific warm modes that the *oscillating simulations* are in. However, for equivalent maximum AMOC strengths, the location of the deep water formation sites and the geometry of the subpolar gyre are clearly distinct between the two different warm modes. This is manifested in the ESPG index and latitude of the SPG COM, which split into two branches for high AMOC indices (Figure 6*c*–*d*). To further describe this phenomenon, we examine the winter and autumn convection layouts and sea ice formations for the two warm modes (Figure 7).

We follow the dynamics of the warm mode shifts by tracking the arrows in Figure 6, omitting in this analysis the initial spin-up period corresponding to values falling outside of the cycles (for example, the first 300 years in *20.7k*). Starting from a *cold* mode, the recovery of the AMOC is first fuelled by convection in the GIN Seas, with very little signal in the Irminger basin, which is covered in sea ice both in Autumn and Winter (Figure 7*a*, *b*, *e*, *f*). This results in a shift eastwards and northwards of the centre of mass of the convection sites, as indicated by a deeper mixed layer (Figure 6*h*). Although situated in an area of intense sea ice formation, the Labrador Sea deep water formation site is not always reactivated during this mode. As a result, the subpolar gyre, which is initially weak and contracted during the *cold* phase, gets slightly stronger and

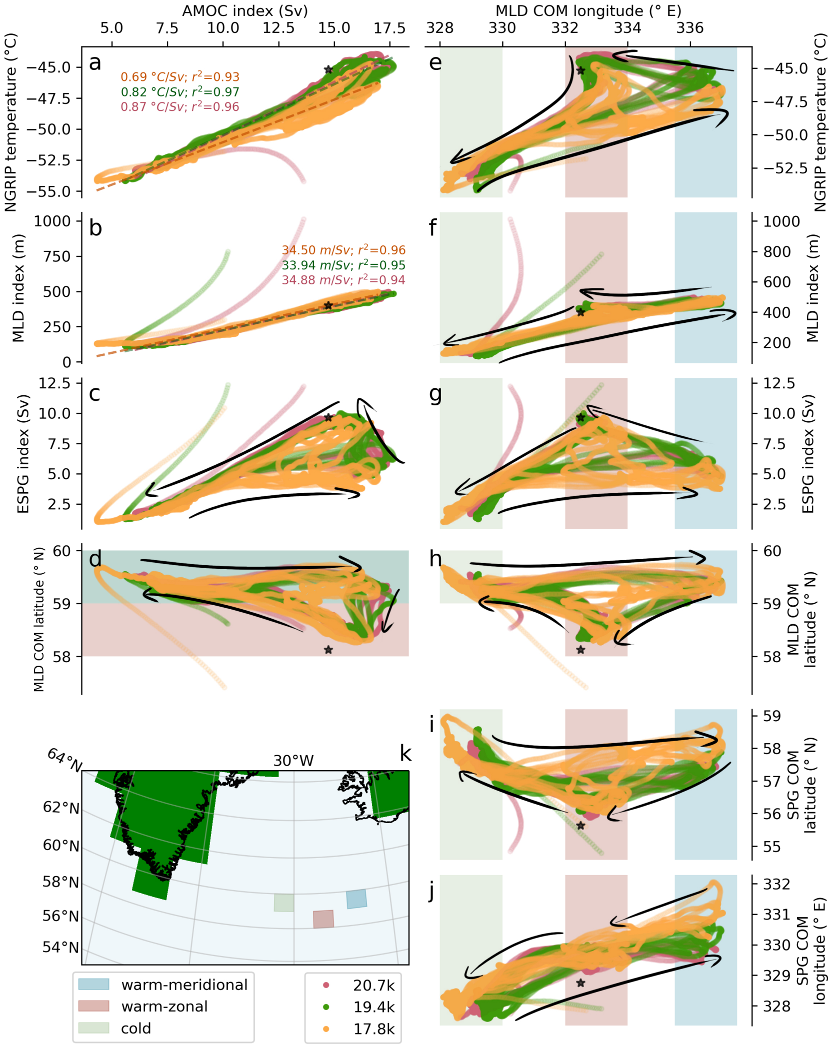

Figure 6. Phase plot of the three *oscillating simulations* showing the relationship between the maximal value of the overturning circulation in the Atlantic ocean at 26.5° N (AMOC index) and *a.* surface air temperature at NGRIP (42.32° W, 75.01° N), *b.* the maximum mixed layer depth in the Northern Hemisphere Atlantic (MLD index), *c.* the mean barotropic stream function in Eastern North Atlantic (ESPG index - see Klockmann et al. (2020) and Figure S9 for zones definition), *d.* the latitude of the centre of mass of the mixed layer depth (MLD COM latitude); and between the longitude of the centre of mass of the mixed layer depth (MLD COM longitude) and *e.* the temperature at NGRIP, *f.* the MLD index, *g.* the ESPG index, *h.* MLD COM latitude, *i.* the latitude of the centre of mass of the barotropic stream function in the subpolar region (SPG COM latitude) and *j.* the longitude of the centre of mass of the barotropic stream function in the subpolar region (SPG COM longitude). The calculation of the centre of mass is detailed in section S8. Colour shading indicates the location of the main areas of activity of the centre of mass of the mixed layer depth during the different modes, as plotted on panel *k.* Arrows indicate the direction of flow (through time) over the phase space; from green (cold) to blue (warm-meridional) to red (warm-zonal) modes. All time series were filtered following the algorithm presented in section S5. The black stars indicate the mean annual values calculated from the last 100-years of *CTRL*.

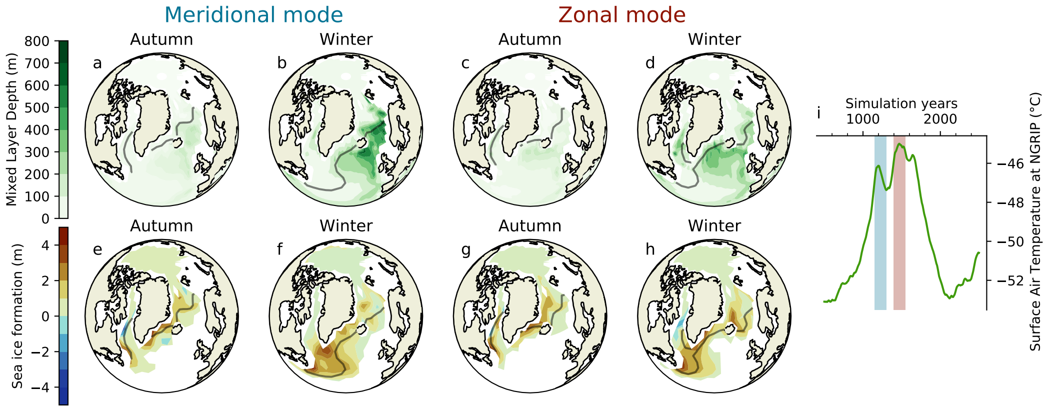

Figure 7. Seasonal Mixed layer depth (panels *a*–*d*) and sea ice formation (panels *e*–*h*) during the meridional (panels *a*, *b*, *e*, *f*) and zonal (panels *c*, *d*, *g*, *h*) warm modes in simulation *19.4k*, defined as the periods indicated in blue and red (respectively) in panel *i*. Autumn (September, October and November) and winter (December, January and February) seasonal means are shown for each variable in each of the two modes. Solid lines indicate the contour for 50% sea-ice concentration. Autumn sea ice formation is defined as the difference between November and September ice depth (in metres) and Winter between February and December. Panel *i* shows the times series of maximum Atlantic overturning circulation at 26° N in the same simulation, identifying the 'meridional' and 'zonal' modes.

extends eastwards (Figure 6*g*, *i*, *j*), entering the *warm-meridional* mode (so labelled for the disposition of the deep water formation sites during this phase). After sustaining a *warm-meridional* state for a few hundred years, the deep water formation layout is disrupted again to return to a state that resembles *CTRL* (comparing Figure 2 to Figure 7*c*–*d*), with convection occurring primarily in the Iceland/Irminger basin and the resumption of Labrador Sea deep water formation in Autumn (Figure 7*c*, *d*, *g*, *h*). The convection is distributed over a larger region and consequently the MLD index slightly dwindles. Conversely, the subpolar gyre intensifies, and moves southward and eastward (Figure 6*i*–*j*). We call this state the *warm-zonal* phase.

Interestingly, we also observe short episodes of AMOC overshoot occurring immediately after the transition from *cold* to *warm-meridional* modes. The overshoots only exist at the onset of *warm-meridional modes* and are associated with stronger convection in the GIN Seas (characterised by a more eastern value of the MLD COM longitude in Figure 7*e*).

Overall, these two *warm* states of strong AMOC are different to the two modes described by Cheng et al. (2011), where there is a transfer of deep water formation across the Atlantic from the the Labrador Sea to the GIN Seas, the latter associated with an AMOC overshot. In all three of *oscillating* simulations, a relatively strong convection is maintained throughout both warm phases of the cycle, and the deep water formation layout only shifts around the Iceland basin.

7 A good example of Dansgaard-Oeschger events?

At first glance, the *oscillating simulations* resemble recorded D-O events. From a purely descriptive point of view, presented in Table 2, we observe a periodicity (defined as the inverse of the dominant frequency in Figure 4) of between 1,540 and 1,930 years (the *18.2k* simulation has a periodicity of 1,290 years, but strictly we do not define this as an *oscillating* simulation). In terms of the duration of D-O cycles, this simulated periodicity is close to the range approximated from palaeo records (about 1,500 years) during times of regular occurrence (Thomas et al., 2009; Lohmann & Ditlevsen, 2019). As an example, we compared our simulated cycles with DO 9-11, which occurred between 44 ka BP and 40 ka BP (Figure 8). This is also very similar to the simulated events of Klockmann et al. (2020) and Armstrong et al. (2022), but two to three times longer than Peltier and Vettoretti (2014). As already discussed, *18.2k* does not qualify as an *oscillating* simulation due to its *slow-recovery* characteristics (section 4). Yet, in Figure 4, we observe two smaller peaks identified by the frequency analysis algorithm, one at $\sim 1{,}300$ years and one at $\sim 3{,}500$ years, which also correspond to typical D-O values (e.g. Kindler et al., 2014).

The temperature ranges between warm and cold climate/AMOC modes are similar, with changes of about 10°C recorded (Huber et al., 2006; Kindler et al., 2014) and simulated (this study) at NGRIP. From the other model studies cited in this study, only Peltier and Vettoretti (2014) obtained a similar amplitude of Greenland temperature change. Both Klockmann et al. (2020) and Armstrong et al. (2022) observed smaller transitions similar more to the 6°C amplitude of *18.2k* oscillations, but still within the lower range of reconstructed D-O events.

Our simulations also show a bipolar see-saw phenomenon (Stocker, 1998; Blunier & Brook, 2001), with a lag between the Northern and Southern Hemisphere temperature changes of around 100 years (Figure 8*a–b*), consistent with the suggestions of Blunier and Brook (2001) and Stocker and Johnsen (2003).

Notwithstanding these similarities with recorded D-O events, because all simulations were realised in a maximum glacial background (specifically, the LGM), the analogy between these simulations and D-O events is not straight forward. This is all the more true as we can also identify significant discrepancies between the model results and observations. For example, the simulated cycles do not match the typical shapes of D-O events (Lohmann & Ditlevsen, 2019); an abrupt warming followed by a slow cooling over a few hundred to a few thousand years within the warm phase followed by a sharper cooling to finish off the cycle. Our simulations displayed a gradual transition between the cold modes to the warm modes, and the strong-AMOC phases were maintained rather steadily for ~500 years before undergoing a slow cooling into the weak-AMOC phase of the cycle (Table 2). The warming and cooling rates are less sharp than palaeo-records suggest, with a typical rate of 3°C temperature change per 100 years, about 10 times slower than indicated in Lohmann and Ditlevsen (2019). It has to be noted that despite a potential damping of the warming and cooling rates due to the filtering, the duration of filtered signals matched the unfiltered ones well, indicating that our conclusion on the shape of the simulated cycles are not an artefact of the analytical method. Using the same model, but simulating an older time period, Armstrong et al. (2022) similarly produced an oscillating ocean/climate with warming rates not exceeding 3°C 100yrs^{-1}, in contrast to the ten times faster faster warming rates simulated by Peltier and Vettoretti (2014) and Klockmann et al. (2020) (their cooling rates overlap with ours).

Presently, we cannot categorically conclude whether or not our oscillations relate to D-O events. Differences in the shape of real and simulated D-O cycles may be explained by the quasi-idealised nature of our experiment design, specifically, the glacial maximum and fixed nature of our climate model boundary conditions/forcings (set to 21 ka, PMIP4 LGM protocol with GLAC-1D ice sheet plus the respective meltwater scenarios from the early deglaciation in GLAC-1D). The framework for our simulations was designed to simplify the identification of different behaviours in response to early deglacial meltwater forcing, mainly inspired by the hypotheses formed in conclusion to earlier work by Ivanovic et al. (2018). It provides a solid and systematic foundation for further work to study the mechanisms at play in the climate simulations presented here. However, this framework

Simulation	Periodicity (ka)	Amplitude (°C)	Warming rate (°C 100yrs^{-1})	Cooling rate (°C 100yrs^{-1})
20.7k	1.54	10.9	4.94	-3.98
19.4k	1.93	8.92	5.19	-3.72
18.2k	1.29	5.90	2.84	-3.57
17.8k	1.67	7.65	4.17	-5.28
Peltier and Vettoretti (2014)	$\sim$ 0.8	$\sim$ 10	$\sim$ 50	$\sim$ -5
Klockmann et al. (2020)	1.5 to 2.0	5 to 6	25 to 50	-5 to -35
Armstrong et al. (2022)	$\sim$ 1.5	6.5 to 8.5	$\sim$ 3	$\sim$ -3

Table 2. Typical oscillation descriptors for the *oscillating* and *slow-recovery* simulations defined from the filtered NGRIP temperature time series (Figure 4) and compared to simulations from Peltier and Vettoretti (2014), Klockmann et al. (2020) and Armstrong et al. (2022). Periodicity was identified using the analysis presented in Figure 4*c*. Amplitude was defined as the difference between the warmest and coldest point of the filtered NGRIP temperature time series Figure 4*b*. Warming and cooling rates were defined as the maximum and minimum of the derivative of the filtered NGRIP temperatures time series, respectively. Descriptors of the simulations performed by Peltier and Vettoretti (2014) were estimated from Figure 1 by Vettoretti and Peltier (2018). Descriptors of the simulations performed by Klockmann et al. (2020) were taken from their main text. Descriptors of the simulations performed by Armstrong et al. (2022) were taken from the main text and estimated from Figure 2 by Armstrong et al. (2022).

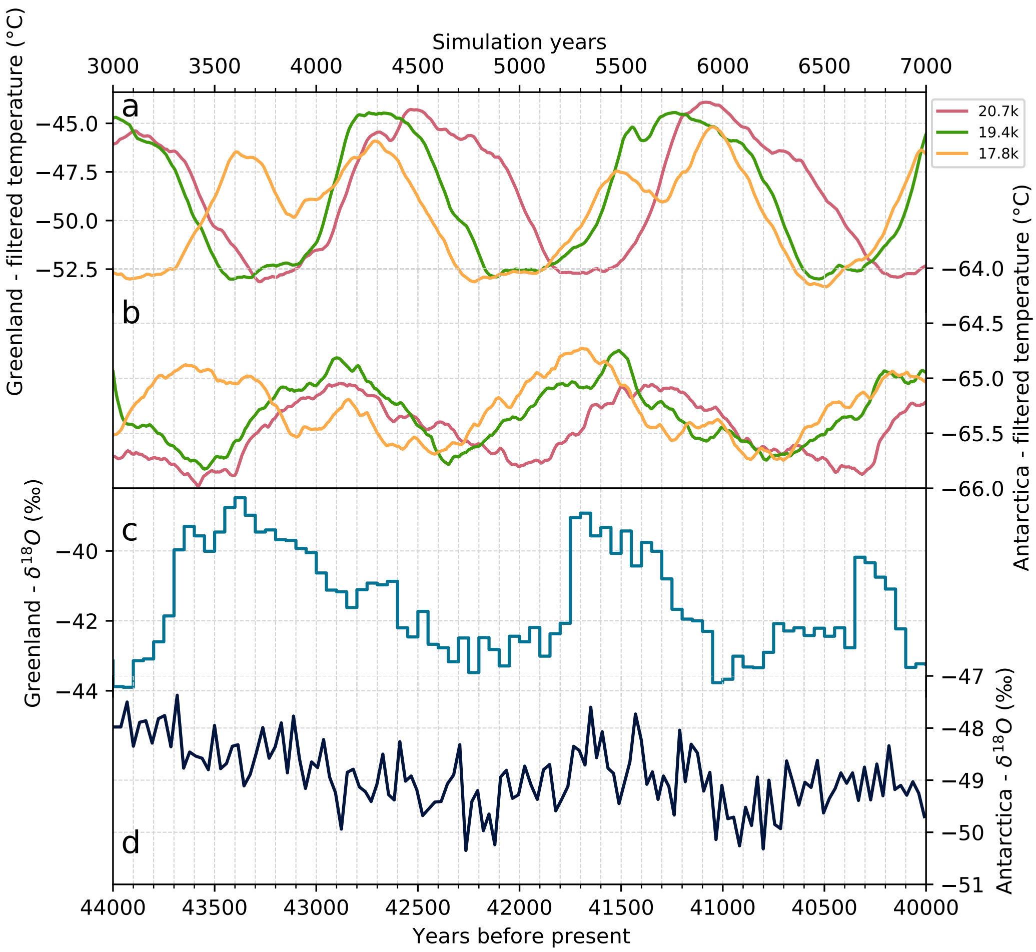

Figure 8. Temporally filtered signals of simulated surface air temperature over *a.* Greenland (NGRIP; 42.32° W, 75.01° N) and *b.* Antarctica (EPICA Dome C; 123.21° E, 75.06° S) for simulation years 3,000 to 7,000. *c.* NGRIP and *d.* EDML (Dronning Maud Land; 0.04° E, 75.00° S) $\delta^{18}O$ records between years 40,000 and 44,000 before present showing DO events 11, 10 and 9, from N.G.R.I.P (2004) and Barbante et al. (2006), respectively.

may interfere with or block some of the complex dynamics of D-O events and damp the abrupt climate changes. We indeed observe the sharpest cooling events at the onset of each simulation, indicating that the initial reorganisation of deep water formation sites in response to a change in freshwater forcing may lead to the strongest and fastest climate disruption. Also, our setup does not include feedbacks between ice sheet melt and temperature changes, which could influence the periodicity of amplitude of changes (Gregoire et al., 2016; Ivanovic et al., 2017). We therefore speculate that implementing a transient meltwater pattern consistent with what is known about past ice sheets during times of abrupt climate change could be a good way to better account for the dynamical interactions and abrupt reorganisations of the earth system, but ultimately, transient coupled climate-ice sheet simulations are needed to fully unlock the challenge of understanding D-O cycles and abrupt deglaical climate change. Finally, the discrepancies between observed D-O cycles and our simulations may also be related to weaknesses in the climate model itself. As concluded by Armstrong et al. (2022), this version of HadCM3 seems to be unable to capture the fast physics component that has been observed in (Vettoretti & Peltier, 2018), and this may be related to the representation of ocean vertical diffusion (Peltier & Vettoretti, 2014).

Furthermore, and specifically to address D-O cycles, we also need to be able to reproduce the phenomenon of oscillating weak-strong AMOC modes outside of a glacial maximum background. Marine Isotope Stage 3 (MIS3, 29–57 ka BP, (Lisiecki & Raymo, 2005), as depicted in Figure 8*c*–*d* for comparison to our results, has been often considered an appropriate candidate for such studies. Stadial conditions then were warmer than at the LGM, and it contains the most regular occurrences of D-O events recorded. Currently, one major challenge for setting off such a suite of simulations is that our oscillations are triggered by meltwater discharge, with a strong dependency on nuanced differences in the rate and location of freshwater inputs to the ocean. Thus, robust and detailed constraints on ice sheet extent are necessary to design an appropriate model experiment.

Apart from Heinrich stadials, MIS3 was not a time when ice sheet melting is thought to have been particularly strong, and there is likely to have been a lower meltwater flux than in our *oscillating simulations* (Hughes et al., 2016; Batchelor et al., 2019). However, DO 15-17 are believed to have been associated with changes of ice sheet extent (Lambeck, 2004), and because their shape remarkably resembles the observed oscillatory cycles of our simulations (Barbante et al., 2006; Rasmussen et al., 2016; Erhardt et al., 2019), they could be good candidates for being triggered by relatively low-levels of Northern Hemisphere ice sheet melt; it is possible that a weaker glacial climate state had a more sensitive ocean to smaller meltwater fluxes than our LGM-based simulations. However, the further back in time we go, the less constrained ice sheet extent (and geometry more broadly) is, which again poses a practical limitation for how well such a climate model experiment could be designed to explore the detail of real past events. In any case, the next step in our investigation of the relationship between our simulations and real DO cycles will be to more deeply understand the physical mechanisms triggered during the model's AMOC and Greenland temperature oscillations.

8 Conclusion

Using snapshots of the meltwater discharge derived from the GLAC-1D ice sheet history of the early last deglaciation, we produced a set of oscillating simulations in the HadCM3 climate model under glacial maximum (PMIP4 LGM) conditions. Switching regularly between cold and warm modes, this behaviour can only be attained in a narrow range of circumstances: if the freshwater forcing is too strong and/or applied in a particularly sensitive part of the ocean, the climate cannot fully recover to a warm mode and stays cold for the majority of the simulation. On the other hand, if the forcing is too weak, the transition to a cold mode is incomplete and the system rebounds to stay permanently in a warm state.

Understanding what can be defined as a 'weak' or 'strong' freshwater flux is not straightforward, as the response to the forcing is non-linear. All simulations are in the range of plausible magnitudes for meltwater discharge over the last deglaciation — although the scenarios are made quasi-idealised by sustaining a constant meltwater discharge over thousands of years rather than following the transient history — but differ significantly in terms of total amplitude, and the geographical distribution of the freshwater fluxes. We identified the release regions closest to the main convection sites, namely the Nordic Seas and the Irminger/Iceland Basins, to be the most sensitive regions to meltwater forcing. One possible inference from this finding is that in spite of being smaller in size compared to the North American ice sheet, Eurasian ice sheet demise punches above its weight in having the potential to trigger abrupt climate changes over the last deglaciation. Conversely, Laurentide ice sheet meltwater is required to be much more substantial to produce similar disruptions to Atlantic Ocean circulation and climate. The impact of the initial climate and ocean state on our results must also be considered. The cold interstadial state obtained with GLAC-1D ice sheets, with a relatively weak AMOC, convection concentrated around Iceland and extensive sea ice in the Western North Atlantic, creates a background that may favour the triggering of abrupt climate changes from Eurasian ice sheet melting.

When reaching a cold mode in our simulations, the ocean and climate response to meltwater forcing becomes decoupled from the direct influence of freshwater input at high latitudes. Because the AMOC is collapsed in these states, and the susceptible North Atlantic deep water formation sites vanished, meltwater perturbations will not propagate any longer, producing only smaller, regional perturbations. Cold modes correspond to an extreme cooling of the North Atlantic, most brutally over former convection regions, with winter sea ice stretching down to Spain. We note a strong consistency in the climate change pattern of all simulations irrespective of whether they belong to the *oscillating*, *slow-recovery*, or, to a lesser extent, *warm* clusters of simulations. This is not true for the warm modes, where the response is very dependent on the meltwater forcing scenario. We observe a range of different AMOC responses, from overshooting to damping, and the resulting climate is very different for each of the simulations. In particular, the simulations dominated by Arctic discharge never manage to completely return to the reference (*CTRL*) state. We also observe a two-phase, bi-modal warm condition in the *oscillating* simulations, with shifts between deep water-formation sites from a more meridional distribution (with primary convection situated in the Nordic seas) to a more zonal configuration comparable to *CTRL*. Resumption of Labrador Sea convection is inconsistent, sometimes being short lived and intense and sometimes being wholly absent, and in these glacial simulations, its connection to the upper cell of the overturning circulation is tenuous.

In summary, while we cannot conclusively determine that the oscillations we simulate are comparable to D-O events, there are resemblances that make such a comparison inviting. D-O events were rarely observed in full-glacial climates and are not believed to be directly forced by changes in ice sheet meltwater discharge. Still, the oscillating simulations presented here offer a valuable framework to analyse further the mechanisms behind the millennial-scale variability in glacial backgrounds. Intriguingly, they provide a set of insightful simulations that are so far unique in that relatively small influxes of freshwater trigger self-sustaining AMOC and Greenland temperature oscillations from glacial *maximum* conditions with a very large LGM North American ice sheet. Finally, the presented simulations pave the way for further study of ice sheet meltwater as a *trigger*, but not a direct *driver*, of abrupt climate changes within the last deglaciation.

9 Data and code availability

The new model data presented here will be available from the University of Leeds Research Data repository upon acceptance of the article. The presented plots realised were produced using the matplotlib python library and some of the colormaps were taken from Crameri et al. (2020). The code is available on github at `https://github.com/Olnavy/ROME2022_paleoceanography_oscillations`, it relies on the packages *pyleaoclim_leeds v1.0* (`https://github.com/Olnavy/pylaeoclim_leeds`) and *mw_protocol v1.0* (`https://github.com/climate-ice/mw_protocol`), also created by the main author.

Acknowledgments

YMR was supported by the Leeds-York-Hull Natural Environment Research Council (NERC) Doctoral Training Partnership (DTP) Panorama under grant NE/S007458/1. LJG was funded by MR/S016961/1 and SST was funded by NE/T007443/1. Simulations were run on the high performance facilities ARC3 and ARC4 at the University of Leeds, UK. All climate and ocean circulation proxy data and model simulations compared to are published elsewhere, with the exception of Armstrong et al. 2022, which is still under review. Thanks are due to CEMAC for technical assistance on the numerical resource, with special thanks to Richard Rigby for assistance with the scripts for managing and processing model output. Thanks to Julia Tindal and Steve Hunter for helpful technical discussions and investigations. Thanks to Kerim Nisancioglu and Chuncheng Guo for insightful discussion about the paper, and to Heather Andres whose presentation at vEGU21 inspired Figure 6.

References

Abe-Ouchi, A., Saito, F., Kageyama, M., Braconnot, P., Harrison, S. P., Lambeck, K., ... Takahashi, K. (2015, November). Ice-sheet configuration in the CMIP5/PMIP3 Last Glacial Maximum experiments. *Geoscientific Model Development*, *8*(11), 3621–3637. Retrieved 2020-03-04, from https://www.geosci-model-dev.net/8/3621/2015/ (Publisher: Copernicus GmbH) doi: https://doi.org/10.5194/gmd-8-3621-2015

Argus, D. F., Peltier, W. R., Drummond, R., & Moore, A. W. (2014, July). The Antarctica component of postglacial rebound model ICE-6G_c (VM5a) based on GPS positioning, exposure age dating of ice thicknesses, and relative sea level histories. *Geophysical Journal International*, *198*(1), 537–563. Retrieved 2020-03-15, from https://academic.oup.com/gji/article/198/1/537/2874192 (Publisher: Oxford Academic) doi: 10.1093/gji/ggu140

Barbante, C., Barnola, J.-M., Becagli, S., Beer, J., Bigler, M., Boutron, C., ... EPICA Community Members (2006, November). One-to-one coupling of glacial climate variability in Greenland and Antarctica. *Nature*, *444*(7116). Retrieved 2021-12-20, from https://www.nature.com/articles/nature05301 doi: 10.1038/nature05301

Barker, S., Chen, J., Gong, X., Jonkers, L., Knorr, G., & Thornalley, D. (2015, April). Icebergs not the trigger for North Atlantic cold events. *Nature*, *520*(7547), 333–336. Retrieved 2019-05-29, from https://www.nature.com/articles/nature14330 doi: 10.1038/nature14330

Barker, S., & Knorr, G. (2021, April). Millennial scale feedbacks determine the shape and rapidity of glacial termination. *Nature Communications*, *12*(1), 2273. Retrieved 2021-09-10, from https://www.nature.com/articles/s41467-021-22388-6 doi: 10.1038/s41467-021-22388-6

Batchelor, C. L., Margold, M., Krapp, M., Murton, D. K., Dalton, A. S., Gibbard, P. L., ... Manica, A. (2019, August). The configuration of Northern Hemisphere ice sheets through the Quaternary. *Nature Communications*, *10*(1), 1–10. Retrieved 2019-09-20, from https://www.nature.com/articles/s41467-019-11601-2 doi: 10.1038/s41467-019-11601-2

Beghin, P., Charbit, S., Dumas, C., Kageyama, M., & Ritz, C. (2015, October). How might the North American ice sheet influence the northwestern Eurasian climate? *Climate of the Past*, *11*(10), 1467–1490. Retrieved 2021-09-08, from https://cp.copernicus.org/articles/11/1467/2015/ (Publisher: Copernicus GmbH) doi: 10.5194/cp-11-1467-2015

Bereiter, B., Eggleston, S., Schmitt, J., Nehrbass-Ahles, C., Stocker, T. F., Fischer, H., ... Chappellaz, J. (2015). Revision of the EPICA Dome C CO2 record from 800 to 600 kyr before present. *Geophysical Research Letters*, *42*(2), 542–549. Retrieved 2020-03-10, from https://agupubs.onlinelibrary.wiley.com/doi/abs/10.1002/2014GL061957 (_eprint: https://agupubs.onlinelibrary.wiley.com/doi/pdf/10.1002/2014GL061957) doi: 10.1002/2014GL061957

Berger, A. (1978, December). Long-Term Variations of Daily Insolation and Quaternary Climatic Changes. *Journal of the Atmospheric Sciences*, *35*(12), 2362–2367. Retrieved 2020-03-10, from https://journals.ametsoc.org/doi/abs/10.1175/1520-0469%281978%29035%3C2362%3ALTVODI%3E2.0.CO%3B2 (Publisher: American Meteorological Society) doi: 10.1175/1520-0469(1978)035⟨2362:LTVODI⟩2.0.CO;2

Bethke, I., Li, C., & Nisancioglu, K. H. (2012). Can we use ice sheet reconstructions to constrain meltwater for deglacial simulations? *Paleoceanography*, *27*(2). Retrieved 2020-03-10, from https://agupubs.onlinelibrary.wiley.com/doi/abs/10.1029/2011PA002258 (_eprint: https://agupubs.onlinelibrary.wiley.com/doi/pdf/10.1029/2011PA002258) doi: 10.1029/2011PA002258

Bigg, G. R., & Wadley, M. R. (2001). Millennial-scale variability in the oceans: an ocean modelling view. *Journal of Quaternary Science*, *16*(4), 309–319. Retrieved 2021-09-06, from `https://onlinelibrary.wiley.com/doi/abs/10.1002/jqs.599` doi: 10.1002/jqs.599

Blunier, T., & Brook, E. J. (2001, January). Timing of Millennial-Scale Climate Change in Antarctica and Greenland During the Last Glacial Period. *Science*, *291*(5501), 109–112. Retrieved 2020-02-26, from `https://science.sciencemag.org/content/291/5501/109` (Publisher: American Association for the Advancement of Science Section: Report) doi: 10.1126/science.291.5501.109

Bond, G., Broecker, W., Johnsen, S., McManus, J., Labeyrie, L., Jouzel, J., & Bonani, G. (1993, September). Correlations between climate records from North Atlantic sediments and Greenland ice. *Nature*, *365*(6442), 143–147. Retrieved 2020-02-26, from `https://www.nature.com/articles/365143a0` (Number: 6442 Publisher: Nature Publishing Group) doi: 10.1038/365143a0

Born, A., & Levermann, A. (2010). The 8.2 ka event: Abrupt transition of the subpolar gyre toward a modern North Atlantic circulation. *Geochemistry, Geophysics, Geosystems*, *11*(6). Retrieved 2019-09-13, from `https://agupubs.pericles-prod.literatumonline.com/doi/abs/10.1029/2009GC003024` doi: 10.1029/2009GC003024

Braconnot, P., Otto-Bliesner, B., Harrison, S., Joussaume, S., Peterchmitt, J.-Y., Abe-Ouchi, A., . . . Zhao, Y. (2007, June). Results of PMIP2 coupled simulations of the Mid-Holocene and Last Glacial Maximum – Part 2: feedbacks with emphasis on the location of the ITCZ and mid- and high latitudes heat budget. *Climate of the Past*, *3*(2), 279–296. Retrieved 2022-02-02, from `https://cp.copernicus.org/articles/3/279/2007/` (Publisher: Copernicus GmbH) doi: 10.5194/cp-3-279-2007

Bradwell, T., Small, D., Fabel, D., Clark, C. D., Chiverrell, R. C., Saher, M. H., . . . Cofaigh, C. O. (2021). Pattern, style and timing of British–Irish Ice Sheet retreat: Shetland and northern North Sea sector. *Journal of Quaternary Science*, *36*(5), 681–722. Retrieved 2021-09-07, from `https://onlinelibrary.wiley.com/doi/abs/10.1002/jqs.3163` (_eprint: https://onlinelibrary.wiley.com/doi/pdf/10.1002/jqs.3163) doi: 10.1002/jqs.3163

Briggs, R. D., Pollard, D., & Tarasov, L. (2014, November). A data-constrained large ensemble analysis of Antarctic evolution since the Eemian. *Quaternary Science Reviews*, *103*, 91–115. Retrieved 2020-03-08, from `http://www.sciencedirect.com/science/article/pii/S0277379114003448` doi: 10.1016/j.quascirev.2014.09.003

Broecker, W. S., Peteet, D. M., & Rind, D. (1985, May). Does the ocean–atmosphere system have more than one stable mode of operation? *Nature*, *315*(6014), 21–26. Retrieved 2020-03-04, from `https://www.nature.com/articles/315021a0` (Number: 6014 Publisher: Nature Publishing Group) doi: 10.1038/315021a0

Brown, N., & Galbraith, E. (2016, August). Hosed vs. unhosed: Interruptions of the Atlantic Meridional Overturning Circulation in a global coupled model, with and without freshwater forcing. *Climate of the Past*, *12*, 1663–1679. doi: 10.5194/cp-12-1663-2016

Bryan, K., & Cox, M. D. (1972, October). An Approximate Equation of State for Numerical Models of Ocean Circulation. *Journal of Physical Oceanography*, *2*(4), 510–514. Retrieved 2021-09-07, from `https://journals.ametsoc.org/view/journals/phoc/2/4/1520-0485_1972_002_0510_aaeosf_2_0_co_2.xml` doi: 10.1175/1520-0485(1972)002⟨0510:AAEOSF⟩2.0.CO;2

Burckel, P., Waelbroeck, C., Gherardi, J. M., Pichat, S., Arz, H., Lippold, J., . . . Thil, F. (2015). Atlantic Ocean circulation changes preceded millennial tropical South America rainfall events during the last glacial. *Geophysical Research Letters*, *42*(2), 411–418. Retrieved 2020-03-04, from https://agupubs.onlinelibrary.wiley.com/doi/abs/10.1002/2014GL062512 (_eprint: https://agupubs.onlinelibrary.wiley.com/doi/pdf/10.1002/2014GL062512) doi: 10.1002/2014GL062512

Böhm, E., Lippold, J., Gutjahr, M., Frank, M., Blaser, P., Antz, B., … Deininger, M. (2015, January). Strong and deep Atlantic meridional overturning circulation during the last glacial cycle. *Nature*, *517*(7532), 73–76. Retrieved 2019-09-20, from https://www.nature.com/articles/nature14059 doi: 10.1038/nature14059

Cheng, J., Liu, Z., He, F., L. Otto-Bliesner, B., Brady, E., & Wehrenberg, M. (2011, January). Simulated Two-Stage Recovery of Atlantic Meridional Overturning Circulation During the Last Deglaciation. *Abrupt Climate Change: Mechanisms, Patterns, and Impacts*, *193*, 75–92. doi: 10.1029/2010gm001014

Clark, P. U., Dyke, A. S., Shakun, J. D., Carlson, A. E., Clark, J., Wohlfarth, B., … McCabe, A. M. (2009, August). The Last Glacial Maximum. *Science*, *325*(5941), 710–714. Retrieved 2020-03-08, from https://science.sciencemag.org/content/325/5941/710 (Publisher: American Association for the Advancement of Science Section: Research Article) doi: 10.1126/science.1172873

Clark, P. U., Pisias, N. G., Stocker, T. F., & Weaver, A. J. (2002, February). The role of the thermohaline circulation in abrupt climate change. *Nature*, *415*(6874), 863–869. Retrieved 2020-03-04, from https://www.nature.com/articles/415863a (Number: 6874 Publisher: Nature Publishing Group) doi: 10.1038/415863a

Condron, A., & Winsor, P. (2012, December). Meltwater routing and the Younger Dryas. *Proceedings of the National Academy of Sciences*, *109*(49), 19928–19933. Retrieved 2020-07-15, from http://www.pnas.org/cgi/doi/10.1073/pnas.1207381109 doi: 10.1073/pnas.1207381109

Cox, P. (2001, January). Description of the TRIFFID dynamic global vegetation model. *Hadley Centre Technical Note*, *24*.

Cox, P. M., Betts, R. A., Bunton, C. B., Essery, R. L. H., Rowntree, P. R., & Smith, J. (1999, March). The impact of new land surface physics on the GCM simulation of climate and climate sensitivity. *Climate Dynamics*, *15*(3), 183–203. Retrieved 2020-07-09, from https://doi.org/10.1007/s003820050276 doi: 10.1007/s003820050276

Crameri, F., Shephard, G. E., & Heron, P. J. (2020, October). The misuse of colour in science communication. *Nature Communications*, *11*(1), 5444. Retrieved 2022-03-18, from https://www.nature.com/articles/s41467-020-19160-7 (Number: 1 Publisher: Nature Publishing Group) doi: 10.1038/s41467-020-19160-7

Dansgaard, W., Johnsen, S. J., Clausen, H. B., Dahl-Jensen, D., Gundestrup, N. S., Hammer, C. U., … Bond, G. (1993, July). Evidence for general instability of past climate from a 250-kyr ice-core record. *Nature*, *364*(6434), 218–220. Retrieved 2019-09-16, from https://www.nature.com/articles/364218a0 doi: 10.1038/364218a0

Davies-Barnard, T., Ridgwell, A., Singarayer, J., & Valdes, P. (2017, October). Quantifying the influence of the terrestrial biosphere on glacial–interglacial climate dynamics. *Climate of the Past*, *13*(10), 1381–1401. Retrieved 2022-03-01, from https://cp.copernicus.org/articles/13/1381/2017/ (Publisher: Copernicus GmbH) doi: 10.5194/cp-13-1381-2017

Dentith, J. E., Ivanovic, R. F., Gregoire, L. J., Tindall, J. C., & Smith, R. S. (2019, February). Ocean circulation drifts in multi-millennial climate simulations: the role of salinity corrections and climate feedbacks. *Climate Dynamics*, *52*(3), 1761–1781. Retrieved 2021-10-28, from https://doi.org/10.1007/

s00382-018-4243-y doi: 10.1007/s00382-018-4243-y

Denton, G. H., Broecker, W. S., & Alley, R. B. (2006, August). The mystery interval 17.5 to 14.5 kyrs ago. *PAGES news*, *14* (2), 14–16. Retrieved 2020-07-15, from http://www.pastglobalchanges.org/products/12189 doi: 10.22498/pages.14.2.14

Dokken, T. M., Nisancioglu, K. H., Li, C., Battisti, D. S., & Kissel, C. (2013). Dansgaard-Oeschger cycles: Interactions between ocean and sea ice intrinsic to the Nordic seas. *Paleoceanography*, *28* (3), 491–502. Retrieved 2019-09-20, from https://agupubs.onlinelibrary.wiley.com/doi/abs/10.1002/palo.20042 doi: 10.1002/palo.20042

Du, J., Haley, B. A., & Mix, A. C. (2020, August). Evolution of the Global Overturning Circulation since the Last Glacial Maximum based on marine authigenic neodymium isotopes. *Quaternary Science Reviews*, *241*, 106396. Retrieved 2022-02-02, from https://www.sciencedirect.com/science/article/pii/S0277379120303589 doi: 10.1016/j.quascirev.2020.106396

Dyke, A. (2004, January). An outline of North American deglaciation with emphasis on central and northern Canada. *Developments in Quaternary Sciences*, *2*, 373–424. Retrieved 2021-04-05, from https://www.sciencedirect.com/science/article/pii/S1571086604802094 (Publisher: Elsevier) doi: 10.1016/S1571-0866(04)80209-4

Erhardt, T., Capron, E., Rasmussen, S. O., Schüpbach, S., Bigler, M., Adolphi, F., & Fischer, H. (2019, April). Decadal-scale progression of the onset of Dansgaard–Oeschger warming events. *Climate of the Past*, *15* (2), 811–825. Retrieved 2021-12-20, from https://cp.copernicus.org/articles/15/811/2019/ (Publisher: Copernicus GmbH) doi: 10.5194/cp-15-811-2019

Fletcher, W. J., Sánchez Goñi, M. F., Allen, J. R. M., Cheddadi, R., Combourieu-Nebout, N., Huntley, B., … Tzedakis, P. C. (2010, October). Millennial-scale variability during the last glacial in vegetation records from Europe. *Quaternary Science Reviews*, *29* (21), 2839–2864. Retrieved 2021-09-06, from https://www.sciencedirect.com/science/article/pii/S0277379109003886 doi: 10.1016/j.quascirev.2009.11.015

Fofonoff, N. P. (1985). Physical properties of seawater: A new salinity scale and equation of state for seawater. *Journal of Geophysical Research: Oceans*, *90* (C2), 3332–3342. Retrieved 2021-09-07, from https://agupubs.onlinelibrary.wiley.com/doi/abs/10.1029/JC090iC02p03332 doi: 10.1029/JC090iC02p03332

Fofonoff, N. P., & Millard Jr, R. C. (1983). Algorithms for the computation of fundamental properties of seawater. *UNESCO Technical Papers in Marine Sciences*. Retrieved 2021-09-07, from https://repository.oceanbestpractices.org/handle/11329/109 doi: 10.25607/OBP-1450

Ganopolski, A., & Rahmstorf, S. (2001, January). Rapid changes of glacial climate simulated in a coupled climate model. *Nature*, *409* (6817), 153–158. Retrieved 2019-09-19, from https://www.nature.com/articles/35051500 doi: 10.1038/35051500

Gebbie, G. (2014). How much did Glacial North Atlantic Water shoal? *Paleoceanography*, *29* (3), 190–209. Retrieved 2021-09-08, from https://agupubs.onlinelibrary.wiley.com/doi/abs/10.1002/2013PA002557 (_eprint: https://agupubs.onlinelibrary.wiley.com/doi/pdf/10.1002/2013PA002557) doi: 10.1002/2013PA002557

Gordon, C., Cooper, C., Senior, C. A., Banks, H., Gregory, J. M., Johns, T. C., … Wood, R. A. (2000, February). The simulation of SST, sea ice extents and ocean heat transports in a version of the Hadley Centre coupled model without flux adjustments. *Climate Dynamics*, *16* (2), 147–168. Retrieved 2020-07-09, from https://doi.org/10.1007/s003820050010 doi: 10.1007/s003820050010

Goñi, M. F. S., Turon, J.-L., Eynaud, F., & Gendreau, S. (2000, November). European Climatic Response to Millennial-Scale Changes in the Atmosphere–Ocean System during the Last Glacial Period. *Quaternary Research*, *54*(3), 394–403. Retrieved 2021-10-26, from https://www.cambridge.org/core/journals/quaternary-research/article/abs/european-climatic-response-to-millennialscale-changes-in-the-atmosphereocean-system-during-the-last-glacial-period/576DB6EF96D6923ED701B117C5939CD0#access-block (Publisher: Cambridge University Press) doi: 10.1006/qres.2000.2176

Gregoire, L. J., Ivanovic, R. F., Maycock, A. C., Valdes, P. J., & Stevenson, S. (2018, November). Holocene lowering of the Laurentide ice sheet affects North Atlantic gyre circulation and climate. *Climate Dynamics*, *51*(9), 3797–3813. Retrieved 2021-02-16, from https://doi.org/10.1007/s00382-018-4111-9 doi: 10.1007/s00382-018-4111-9

Gregoire, L. J., Otto-Bliesner, B., Valdes, P. J., & Ivanovic, R. (2016). Abrupt Bølling warming and ice saddle collapse contributions to the Meltwater Pulse 1a rapid sea level rise. *Geophysical Research Letters*, *43*(17), 9130–9137. Retrieved 2022-03-04, from https://onlinelibrary.wiley.com/doi/abs/10.1002/2016GL070356 (_eprint: https://onlinelibrary.wiley.com/doi/pdf/10.1002/2016GL070356) doi: 10.1002/2016GL070356

Gregoire, L. J., Payne, A. J., & Valdes, P. J. (2012, July). Deglacial rapid sea level rises caused by ice-sheet saddle collapses. *Nature*, *487*(7406), 219–222. Retrieved 2020-03-15, from https://www.nature.com/articles/nature11257 (Number: 7406 Publisher: Nature Publishing Group) doi: 10.1038/nature11257

Gregoire, L. J., Valdes, P. J., & Payne, A. J. (2015). The relative contribution of orbital forcing and greenhouse gases to the North American deglaciation. *Geophysical Research Letters*, *42*(22), 9970–9979. Retrieved 2020-03-16, from https://agupubs.onlinelibrary.wiley.com/doi/abs/10.1002/2015GL066005 (_eprint: https://agupubs.onlinelibrary.wiley.com/doi/pdf/10.1002/2015GL066005) doi: 10.1002/2015GL066005

Guo, C., Nisancioglu, K. H., Bentsen, M., Bethke, I., & Zhang, Z. (2019, June). Equilibrium simulations of Marine Isotope Stage 3 climate. *Climate of the Past*, *15*(3), 1133–1151. Retrieved 2020-05-11, from https://www.clim-past.net/15/1133/2019/ (Publisher: Copernicus GmbH) doi: https://doi.org/10.5194/cp-15-1133-2019

Heinrich, H. (1988, March). Origin and consequences of cyclic ice rafting in the Northeast Atlantic Ocean during the past 130,000 years. *Quaternary Research*, *29*(2), 142–152. Retrieved 2019-09-16, from http://www.sciencedirect.com/science/article/pii/0033589488900579 doi: 10.1016/0033-5894(88)90057-9

Hemming, S. R. (2004, March). Heinrich events: Massive late Pleistocene detritus layers of the North Atlantic and their global climate imprint. *Reviews of Geophysics*, *42*(1). Retrieved 2019-08-27, from https://agupubs.onlinelibrary.wiley.com/doi/full/10.1029/2003RG000128 doi: 10.1029/2003RG000128

Henry, L. G., McManus, J. F., Curry, W. B., Roberts, N. L., Piotrowski, A. M., & Keigwin, L. D. (2016, July). North Atlantic ocean circulation and abrupt climate change during the last glaciation. *Science*, *353*(6298), 470–474. Retrieved 2020-03-04, from https://science.sciencemag.org/content/353/6298/470 (Publisher: American Association for the Advancement of Science Section: Report) doi: 10.1126/science.aaf5529

Hodell, D. A., Nicholl, J. A., Bontognali, T. R. R., Danino, S., Dorador, J., Dowdeswell, J. A., . . . Röhl, U. (2017). Anatomy of Heinrich Layer 1 and its role in the last deglaciation. *Paleoceanography*, *32*(3), 284–303. Retrieved

2020-07-15, from https://agupubs.onlinelibrary.wiley.com/doi/abs/10.1002/2016PA003028 doi: 10.1002/2016PA003028

Huber, C., Leuenberger, M., Spahni, R., Flückiger, J., Schwander, J., Stocker, T. F., ... Jouzel, J. (2006, March). Isotope calibrated Greenland temperature record over Marine Isotope Stage 3 and its relation to CH4. *Earth and Planetary Science Letters*, *243*(3), 504–519. Retrieved 2020-06-29, from http://www.sciencedirect.com/science/article/pii/S0012821X06000392 doi: 10.1016/j.epsl.2006.01.002

Hughes, A. L. C., Gyllencreutz, R., Lohne, Ø. S., Mangerud, J., & Svendsen, J. I. (2016). The last Eurasian ice sheets – a chronological database and time-slice reconstruction, DATED-1. *Boreas*, *45*(1), 1–45. Retrieved 2020-01-27, from https://onlinelibrary.wiley.com/doi/abs/10.1111/bor.12142 doi: 10.1111/bor.12142

I.P.C.C. (2014). Evaluation of Climate Models. In Intergovernmental Panel on Climate Change (Ed.), *Climate Change 2013 – The Physical Science Basis: Working Group I Contribution to the Fifth Assessment Report of the Intergovernmental Panel on Climate Change* (pp. 741–866). Cambridge: Cambridge University Press. Retrieved 2021-09-06, from https://www.cambridge.org/core/books/climate-change-2013-the-physical-science-basis/evaluation-of-climate-models/94BC2268C864F2C6A18436DB22BD1E5A doi: 10.1017/CBO9781107415324.020

Ivanovic, R. F., Gregoire, L. J., Burke, A., Wickert, A. D., Valdes, P. J., Ng, H. C., ... Dentith, J. E. (2018). Acceleration of Northern Ice Sheet Melt Induces AMOC Slowdown and Northern Cooling in Simulations of the Early Last Deglaciation. *Paleoceanography and Paleoclimatology*, *33*(7), 807–824. Retrieved 2019-10-02, from https://agupubs.onlinelibrary.wiley.com/doi/abs/10.1029/2017PA003308 doi: 10.1029/2017PA003308

Ivanovic, R. F., Gregoire, L. J., Kageyama, M., Roche, D. M., Valdes, P. J., Burke, A., ... Tarasov, L. (2016, July). Transient climate simulations of the deglaciation 21–9 thousand years before present (version 1) – PMIP4 Core experiment design and boundary conditions. *Geoscientific Model Development*, *9*(7), 2563–2587. Retrieved 2020-02-20, from https://www.geosci-model-dev.net/9/2563/2016/ doi: https://doi.org/10.5194/gmd-9-2563-2016

Ivanovic, R. F., Gregoire, L. J., Wickert, A. D., Valdes, P. J., & Burke, A. (2017). Collapse of the North American ice saddle 14,500 years ago caused widespread cooling and reduced ocean overturning circulation. *Geophysical Research Letters*, *44*(1), 383–392. Retrieved 2020-07-09, from https://agupubs.onlinelibrary.wiley.com/doi/abs/10.1002/2016GL071849 (_eprint: https://agupubs.onlinelibrary.wiley.com/doi/pdf/10.1002/2016GL071849) doi: 10.1002/2016GL071849

Kageyama, M., Albani, S., Braconnot, P., Harrison, S. P., Hopcroft, P. O., Ivanovic, R. F., ... Zheng, W. (2017, November). The PMIP4 contribution to CMIP6 – Part 4: Scientific objectives and experimental design of the PMIP4-CMIP6 Last Glacial Maximum experiments and PMIP4 sensitivity experiments. *Geoscientific Model Development*, *10*(11), 4035–4055. Retrieved 2020-02-20, from https://www.geosci-model-dev.net/10/4035/2017/ doi: https://doi.org/10.5194/gmd-10-4035-2017

Kageyama, M., Harrison, S. P., Kapsch, M.-L., Lofverstrom, M., Lora, J. M., Mikolajewicz, U., ... Zhu, J. (2021, May). The PMIP4 Last Glacial Maximum experiments: preliminary results and comparison with the PMIP3 simulations. *Climate of the Past*, *17*(3), 1065–1089. Retrieved 2022-03-01, from https://cp.copernicus.org/articles/17/1065/2021/ (Publisher: Copernicus GmbH) doi: 10.5194/cp-17-1065-2021

Kageyama, M., Paul, A., Roche, D. M., & Van Meerbeeck, C. J. (2010, October). Modelling glacial climatic millennial-scale variability related to changes in the Atlantic meridional overturning circulation: a review. *Quaternary Science Reviews*, *29*(21), 2931–2956. Retrieved 2020-03-05, from http://www.sciencedirect.com/science/article/pii/S0277379110001745 doi: 10.1016/j.quascirev.2010.05.029

Kapsch, M.-L., Mikolajewicz, U., Ziemen, F., & Schannwell, C. (2022). Ocean response in transient simulations of the last deglaciation dominated by underlying ice-sheet reconstruction and method of meltwater distribution. *Geophysical Research Letters*, *n/a*(n/a), e2021GL096767. Retrieved 2022-02-02, from https://onlinelibrary.wiley.com/doi/abs/10.1029/2021GL096767 doi: 10.1029/2021GL096767

Kindler, P., Guillevic, M., Baumgartner, M., Schwander, J., Landais, A., & Leuenberger, M. (2014, April). Temperature reconstruction from 10 to 120 kyr b2k from the NGRIP ice core. *Climate of the Past*, *10*(2), 887–902. Retrieved 2021-02-10, from https://cp.copernicus.org/articles/10/887/2014/cp-10-887-2014.html (Publisher: Copernicus GmbH) doi: https://doi.org/10.5194/cp-10-887-2014

Klockmann, M., Mikolajewicz, U., Kleppin, H., & Marotzke, J. (2020). Coupling of the Subpolar Gyre and the Overturning Circulation During Abrupt Glacial Climate Transitions. *Geophysical Research Letters*, *47*(21), e2020GL090361. Retrieved 2020-12-11, from https://agupubs.onlinelibrary.wiley.com/doi/abs/10.1029/2020GL090361 (_eprint: https://agupubs.onlinelibrary.wiley.com/doi/pdf/10.1029/2020GL090361) doi: https://doi.org/10.1029/2020GL090361

Klockmann, M., Mikolajewicz, U., & Marotzke, J. (2016, September). The effect of greenhouse gas concentrations and ice sheets on the glacial AMOC in a coupled climate model. *Climate of the Past*, *12*(9), 1829–1846. Retrieved 2021-09-08, from https://cp.copernicus.org/articles/12/1829/2016/ (Publisher: Copernicus GmbH) doi: 10.5194/cp-12-1829-2016

Klockmann, M., Mikolajewicz, U., & Marotzke, J. (2018, July). Two AMOC States in Response to Decreasing Greenhouse Gas Concentrations in the Coupled Climate Model MPI-ESM. *Journal of Climate*, *31*(19), 7969–7984. Retrieved 2019-10-02, from https://journals.ametsoc.org/doi/full/10.1175/JCLI-D-17-0859.1 doi: 10.1175/JCLI-D-17-0859.1

Lambeck, K. (2004, June). Sea-level change through the last glacial cycle: geophysical, glaciological and palaeogeographic consequences. *Comptes Rendus Geoscience*, *336*(7), 677–689. Retrieved 2021-12-20, from https://www.sciencedirect.com/science/article/pii/S1631071304000896 doi: 10.1016/j.crte.2003.12.017

Lambeck, K., Rouby, H., Purcell, A., Sun, Y., & Sambridge, M. (2014, October). Sea level and global ice volumes from the Last Glacial Maximum to the Holocene. *Proceedings of the National Academy of Sciences*, *111*(43), 15296–15303. Retrieved 2020-12-11, from https://www.pnas.org/content/111/43/15296 (Publisher: National Academy of Sciences Section: Physical Sciences) doi: 10.1073/pnas.1411762111

Li, C., & Born, A. (2019, January). Coupled atmosphere-ice-ocean dynamics in Dansgaard-Oeschger events. *Quaternary Science Reviews*, *203*, 1–20. Retrieved 2020-02-20, from http://www.sciencedirect.com/science/article/pii/S0277379118305705 doi: 10.1016/j.quascirev.2018.10.031

Lisiecki, L. E., & Raymo, M. E. (2005). A Pliocene-Pleistocene stack of 57 globally distributed benthic $\delta^{18}o$ records. *Paleoceanography*, *20*(1). Retrieved 2020-03-13, from https://agupubs.onlinelibrary.wiley.com/doi/abs/10.1029/2004PA001071 (_eprint: https://agupubs.onlinelibrary.wiley.com/doi/pdf/10.1029/2004PA001071) doi: 10.1029/2004PA001071

Liu, Z., Carlson, A. E., He, F., Brady, E. C., Otto-Bliesner, B. L., Briegleb, B. P.,

... Zhu, J. (2012, July). Younger Dryas cooling and the Greenland climate response to CO2. *Proceedings of the National Academy of Sciences*, *109*(28), 11101–11104. Retrieved 2020-03-15, from https://www.pnas.org/content/109/28/11101 (Publisher: National Academy of Sciences Section: Physical Sciences) doi: 10.1073/pnas.1202183109

Liu, Z., Otto-Bliesner, B. L., He, F., Brady, E. C., Tomas, R., Clark, P. U., ... Cheng, J. (2009, July). Transient Simulation of Last Deglaciation with a New Mechanism for Bølling-Allerød Warming. *Science*, *325*(5938), 310–314. Retrieved 2019-10-02, from https://science.sciencemag.org/content/325/5938/310 doi: 10.1126/science.1171041

Lohmann, J., & Ditlevsen, P. D. (2019, September). Objective extraction and analysis of statistical features of Dansgaard–Oeschger events. *Climate of the Past*, *15*(5), 1771–1792. Retrieved 2021-01-28, from https://cp.copernicus.org/articles/15/1771/2019/ (Publisher: Copernicus GmbH) doi: https://doi.org/10.5194/cp-15-1771-2019

Loulergue, L., Schilt, A., Spahni, R., Masson-Delmotte, V., Blunier, T., Lemieux, B., ... Chappellaz, J. (2008, May). Orbital and millennial-scale features of atmospheric CH 4 over the past 800,000 years. *Nature*, *453*(7193), 383–386. Retrieved 2020-03-10, from https://www.nature.com/articles/nature06950 (Number: 7193 Publisher: Nature Publishing Group) doi: 10.1038/nature06950

Lynch-Stieglitz, J. (2017, January). The Atlantic Meridional Overturning Circulation and Abrupt Climate Change. *Annual Review of Marine Science*, *9*(1), 83–104. Retrieved 2020-03-04, from https://www.annualreviews.org/doi/10.1146/annurev-marine-010816-060415 (Publisher: Annual Reviews) doi: 10.1146/annurev-marine-010816-060415

Löfverström, M., Caballero, R., Nilsson, J., & Kleman, J. (2014, July). Evolution of the large-scale atmospheric circulation in response to changing ice sheets over the last glacial cycle. *Climate of the Past*, *10*(4), 1453–1471. Retrieved 2022-02-02, from https://cp.copernicus.org/articles/10/1453/2014/ (Publisher: Copernicus GmbH) doi: 10.5194/cp-10-1453-2014

Manabe, S., & Stouffer, R. J. (1988, September). Two Stable Equilibria of a Coupled Ocean-Atmosphere Model. *Journal of Climate*, *1*(9), 841–866. Retrieved 2020-03-04, from https://journals.ametsoc.org/doi/abs/10.1175/1520-0442%281988%29001%3C0841%3ATSEOAC%3E2.0.CO%3B2 (Publisher: American Meteorological Society) doi: 10.1175/1520-0442(1988)001⟨0841:TSEOAC⟩2.0.CO;2

Manabe, S., & Stouffer, R. J. (1997). Coupled ocean-atmosphere model response to freshwater input: Comparison to Younger Dryas Event. *Paleoceanography*, *12*(2), 321–336. Retrieved 2020-03-08, from https://agupubs.onlinelibrary.wiley.com/doi/abs/10.1029/96PA03932 doi: 10.1029/96PA03932

Margari, V., Gibbard, P. L., Bryant, C. L., & Tzedakis, P. C. (2009, June). Character of vegetational and environmental changes in southern Europe during the last glacial period; evidence from Lesvos Island, Greece. *Quaternary Science Reviews*, *28*(13), 1317–1339. Retrieved 2021-10-26, from https://www.sciencedirect.com/science/article/pii/S0277379109000353 doi: 10.1016/j.quascirev.2009.01.008

Marzocchi, A., & Jansen, M. F. (2017, June). Connecting Antarctic sea ice to deep-ocean circulation in modern and glacial climate simulations. *Geophysical Research Letters*, *44*(12), 6286–6295. Retrieved 2021-12-17, from https://agupubs.onlinelibrary.wiley.com/doi/10.1002/2017GL073936 (Publisher: John Wiley & Sons, Ltd) doi: 10.1002/2017GL073936

Matero, I. S. O., Gregoire, L. J., Ivanovic, R. F., Tindall, J. C., & Haywood, A. M. (2017, September). The 8.2 ka cooling event caused by Laurentide ice saddle collapse. *Earth and Planetary Science Letters*, *473*, 205–214. Retrieved

2021-09-06, from https://www.sciencedirect.com/science/article/pii/S0012821X17303205 doi: 10.1016/j.epsl.2017.06.011

Menviel, L., Timmermann, A., Timm, O. E., & Mouchet, A. (2011, May). Deconstructing the Last Glacial termination: the role of millennial and orbital-scale forcings. *Quaternary Science Reviews*, *30*(9), 1155–1172. Retrieved 2020-03-16, from http://www.sciencedirect.com/science/article/pii/S0277379111000539 doi: 10.1016/j.quascirev.2011.02.005

Muglia, J., & Schmittner, A. (2015). Glacial Atlantic overturning increased by wind stress in climate models. *Geophysical Research Letters*, *42*(22), 9862–9868. Retrieved 2019-09-16, from https://agupubs.onlinelibrary.wiley.com/doi/abs/10.1002/2015GL064583 doi: 10.1002/2015GL064583

Muglia, J., & Schmittner, A. (2021, April). Carbon isotope constraints on glacial Atlantic meridional overturning: Strength vs depth. *Quaternary Science Reviews*, *257*, 106844. Retrieved 2021-10-26, from https://www.sciencedirect.com/science/article/pii/S0277379121000512 doi: 10.1016/j.quascirev.2021.106844

Murton, J. B., Bateman, M. D., Dallimore, S. R., Teller, J. T., & Yang, Z. (2010, April). Identification of Younger Dryas outburst flood path from Lake Agassiz to the Arctic Ocean. *Nature*, *464*(7289), 740–743. Retrieved 2020-03-15, from https://www.nature.com/articles/nature08954 (Number: 7289 Publisher: Nature Publishing Group) doi: 10.1038/nature08954

Ng, H. C., Robinson, L. F., McManus, J. F., Mohamed, K. J., Jacobel, A. W., Ivanovic, R. F., ... Chen, T. (2018, July). Coherent deglacial changes in western Atlantic Ocean circulation. *Nature Communications*, *9*(1), 1–10. Retrieved 2019-10-02, from https://www.nature.com/articles/s41467-018-05312-3 doi: 10.1038/s41467-018-05312-3

N.G.R.I.P, M. (2004, September). High-resolution record of Northern Hemisphere climate extending into the last interglacial period. *Nature*, *431*(7005), 147–151. Retrieved 2020-03-13, from https://www.nature.com/articles/nature02805 (Number: 7005 Publisher: Nature Publishing Group) doi: 10.1038/nature02805

Obase, T., & Abe-Ouchi, A. (2019). Abrupt Bølling-Allerød Warming Simulated under Gradual Forcing of the Last Deglaciation. *Geophysical Research Letters*, *46*(20), 11397–11405. Retrieved 2021-12-17, from https://onlinelibrary.wiley.com/doi/abs/10.1029/2019GL084675 doi: 10.1029/2019GL084675

Oka, A., Hasumi, H., & Abe-Ouchi, A. (2012). The thermal threshold of the Atlantic meridional overturning circulation and its control by wind stress forcing during glacial climate. *Geophysical Research Letters*, *39*(9). Retrieved 2021-09-08, from https://agupubs.onlinelibrary.wiley.com/doi/abs/10.1029/2012GL051421 (_eprint: https://agupubs.onlinelibrary.wiley.com/doi/pdf/10.1029/2012GL051421) doi: 10.1029/2012GL051421

Osman, M. B., Tierney, J. E., Zhu, J., Tardif, R., Hakim, G. J., King, J., & Poulsen, C. J. (2021, November). Globally resolved surface temperatures since the Last Glacial Maximum. *Nature*, *599*(7884), 239–244. Retrieved 2021-12-19, from https://www.nature.com/articles/s41586-021-03984-4 doi: 10.1038/s41586-021-03984-4

Paillard, D., & Labeyriet, L. (1994, November). Role of the thermohaline circulation in the abrupt warming after Heinrich events. *Nature*, *372*(6502), 162–164. Retrieved 2020-02-28, from https://www.nature.com/articles/372162a0 (Number: 6502 Publisher: Nature Publishing Group) doi: 10.1038/372162a0

Parrenin, F., Barnola, J.-M., Beer, J., Blunier, T., Castellano, E., Chappellaz, J., ... Wolff, E. (2007, August). The EDC3 chronology for the EPICA Dome C ice core. *Climate of the Past*, *3*(3), 485–497. Retrieved 2020-07-15, from https://cp.copernicus.org/articles/3/485/2007/ (Publisher: Copernicus GmbH) doi: https://doi.org/10.5194/cp-3-485-2007

Paul, A., Mulitza, S., Stein, R., & Werner, M. (2021, April). A global climatology of the ocean surface during the Last Glacial Maximum mapped on a regular grid (GLOMAP). *Climate of the Past*, *17*(2), 805–824. Retrieved 2021-12-19, from https://cp.copernicus.org/articles/17/805/2021/ (Publisher: Copernicus GmbH) doi: 10.5194/cp-17-805-2021

Peltier, W. R., Argus, D. F., & Drummond, R. (2015). Space geodesy constrains ice age terminal deglaciation: The global ICE-6G_c (VM5a) model. *Journal of Geophysical Research: Solid Earth*, *120*(1), 450–487. Retrieved 2020-03-08, from https://agupubs.onlinelibrary.wiley.com/doi/abs/10.1002/2014JB011176 (_eprint: https://agupubs.onlinelibrary.wiley.com/doi/pdf/10.1002/2014JB011176) doi: 10.1002/2014JB011176

Peltier, W. R., & Vettoretti, G. (2014). Dansgaard-Oeschger oscillations predicted in a comprehensive model of glacial climate: A "kicked" salt oscillator in the Atlantic. *Geophysical Research Letters*, *41*(20), 7306–7313. Retrieved 2019-08-05, from https://agupubs.onlinelibrary.wiley.com/doi/abs/10.1002/2014GL061413 doi: 10.1002/2014GL061413

Peterson, L. C., & Haug, G. H. (2006, May). Variability in the mean latitude of the Atlantic Intertropical Convergence Zone as recorded by riverine input of sediments to the Cariaco Basin (Venezuela). *Palaeogeography, Palaeoclimatology, Palaeoecology*, *234*(1), 97–113. Retrieved 2022-03-01, from https://www.sciencedirect.com/science/article/pii/S0031018205006115 doi: 10.1016/j.palaeo.2005.10.021

Pope, V. D., Gallani, M. L., Rowntree, P. R., & Stratton, R. A. (2000, February). The impact of new physical parametrizations in the Hadley Centre climate model: HadAM3. *Climate Dynamics*, *16*(2), 123–146. Retrieved 2020-07-09, from https://doi.org/10.1007/s003820050009 doi: 10.1007/s003820050009

Rahmstorf, S. (2002, September). Ocean circulation and climate during the past 120,000 years. *Nature*, *419*(6903), 207–214. Retrieved 2020-03-04, from https://www.nature.com/articles/nature01090 (Number: 6903 Publisher: Nature Publishing Group) doi: 10.1038/nature01090

Rasmussen, T. L., Thomsen, E., & Moros, M. (2016, February). North Atlantic warming during Dansgaard-Oeschger events synchronous with Antarctic warming and out-of-phase with Greenland climate. *Scientific Reports*, *6*(1), 20535. Retrieved 2020-07-13, from https://www.nature.com/articles/srep20535 (Number: 1 Publisher: Nature Publishing Group) doi: 10.1038/srep20535

Reichler, T., & Kim, J. (2008, March). How Well Do Coupled Models Simulate Today's Climate? *Bulletin of the American Meteorological Society*, *89*(3), 303–312. Retrieved 2021-09-06, from https://journals.ametsoc.org/view/journals/bams/89/3/bams-89-3-303.xml (Publisher: American Meteorological Society Section: Bulletin of the American Meteorological Society) doi: 10.1175/BAMS-89-3-303

Renold, M., Raible, C. C., Yoshimori, M., & Stocker, T. F. (2010, January). Simulated resumption of the North Atlantic meridional overturning circulation – Slow basin-wide advection and abrupt local convection. *Quaternary Science Reviews*, *29*(1), 101–112. Retrieved 2019-05-29, from http://www.sciencedirect.com/science/article/pii/S0277379109003680 doi: 10.1016/j.quascirev.2009.11.005

Roberts, W. H. G., & Valdes, P. J. (2017, May). Green Mountains and White Plains: The Effect of Northern Hemisphere Ice Sheets on the Global Energy Budget. *Journal of Climate*, *30*(10), 3887–3905. Retrieved 2020-06-29, from https://journals.ametsoc.org/jcli/article/30/10/3887/106888/

Green-Mountains-and-White-Plains-The-Effect-of (Publisher: American Meteorological Society) doi: 10.1175/JCLI-D-15-0846.1

Roberts, W. H. G., Valdes, P. J., & Payne, A. J. (2014, November). Topography's crucial role in Heinrich Events. *Proceedings of the National Academy of Sciences*, *111*(47), 16688–16693. Retrieved 2020-07-13, from https://www.pnas.org/content/111/47/16688 (Publisher: National Academy of Sciences Section: Physical Sciences) doi: 10.1073/pnas.1414882111

Roche, D. M., Renssen, H., Paillard, D., & Levavasseur, G. (2011, June). Deciphering the spatio-temporal complexity of climate change of the last deglaciation: a model analysis. *Climate of the Past*, *7*(2), 591–602. Retrieved 2020-03-16, from https://www.clim-past.net/7/591/2011/ (Publisher: Copernicus GmbH) doi: https://doi.org/10.5194/cp-7-591-2011

Roche, D. M., Wiersma, A. P., & Renssen, H. (2010, June). A systematic study of the impact of freshwater pulses with respect to different geographical locations. *Climate Dynamics*, *34*(7), 997–1013. Retrieved 2019-05-29, from https://doi.org/10.1007/s00382-009-0578-8 doi: 10.1007/s00382-009-0578-8

Schilt, A., Baumgartner, M., Schwander, J., Buiron, D., Capron, E., Chappellaz, J., ... Stocker, T. F. (2010, November). Atmospheric nitrous oxide during the last 140,000years. *Earth and Planetary Science Letters*, *300*(1), 33–43. Retrieved 2020-03-10, from http://www.sciencedirect.com/science/article/pii/S0012821X10006023 doi: 10.1016/j.epsl.2010.09.027

Schmittner, A., Yoshimori, M., & Weaver, A. J. (2002, February). Instability of Glacial Climate in a Model of the Ocean- Atmosphere-Cryosphere System. *Science*, *295*(5559), 1489–1493. Retrieved 2020-03-08, from https://science.sciencemag.org/content/295/5559/1489 (Publisher: American Association for the Advancement of Science Section: Research Article) doi: 10.1126/science.1066174

Severinghaus, J. P., & Brook, E. J. (1999, October). Abrupt Climate Change at the End of the Last Glacial Period Inferred from Trapped Air in Polar Ice. *Science*, *286*(5441), 930–934. Retrieved 2020-03-10, from https://science.sciencemag.org/content/286/5441/930 (Publisher: American Association for the Advancement of Science Section: Report) doi: 10.1126/science.286.5441.930

Shackleton, N. J., Hall, M. A., & Vincent, E. (2000). Phase relationships between millennial-scale events 64,000–24,000 years ago. *Paleoceanography*, *15*(6), 565–569. Retrieved 2020-03-04, from https://agupubs.onlinelibrary.wiley.com/doi/abs/10.1029/2000PA000513 (_eprint: https://agupubs.onlinelibrary.wiley.com/doi/pdf/10.1029/2000PA000513) doi: 10.1029/2000PA000513

Sherriff-Tadano, S., & Abe-Ouchi, A. (2020, April). Roles of Sea Ice–Surface Wind Feedback in Maintaining the Glacial Atlantic Meridional Overturning Circulation and Climate. *Journal of Climate*, *33*(8), 3001–3018. Retrieved 2022-03-01, from https://journals.ametsoc.org/view/journals/clim/33/8/jcli-d-19-0431.1.xml (Publisher: American Meteorological Society Section: Journal of Climate) doi: 10.1175/JCLI-D-19-0431.1

Sherriff-Tadano, S., Abe-Ouchi, A., & Oka, A. (2021, January). Impact of mid-glacial ice sheets on deep ocean circulation and global climate. *Climate of the Past*, *17*(1), 95–110. Retrieved 2022-03-01, from https://cp.copernicus.org/articles/17/95/2021/ (Publisher: Copernicus GmbH) doi: 10.5194/cp-17-95-2021

Sherriff-Tadano, S., Abe-Ouchi, A., Yoshimori, M., Oka, A., & Chan, W.-L. (2018, April). Influence of glacial ice sheets on the Atlantic meridional overturning circulation through surface wind change. *Climate Dynamics*, *50*(7), 2881–2903. Retrieved 2019-08-19, from https://doi.org/10.1007/s00382-017-3780-0 doi: 10.1007/s00382-017-3780-0

Singarayer, J. S., Valdes, P. J., & Roberts, W. H. G. (2017, August). Ocean dominated expansion and contraction of the late Quaternary tropical rainbelt. *Scientific Reports*, *7*(1), 9382. Retrieved 2022-01-21, from https://www.nature.com/articles/s41598-017-09816-8 doi: 10.1038/s41598-017-09816-8

Smeed, D. A., McCarthy, G. D., Cunningham, S. A., Frajka-Williams, E., Rayner, D., Johns, W. E., ... Bryden, H. L. (2014, February). Observed decline of the Atlantic meridional overturning circulation 2004–2012. *Ocean Science*, *10*(1), 29–38. Retrieved 2020-02-27, from https://www.ocean-sci.net/10/29/2014/ doi: https://doi.org/10.5194/os-10-29-2014

Smith, R. S., & Gregory, J. M. (2009). A study of the sensitivity of ocean overturning circulation and climate to freshwater input in different regions of the North Atlantic. *Geophysical Research Letters*, *36*(15). Retrieved 2022-02-02, from https://onlinelibrary.wiley.com/doi/abs/10.1029/2009GL038607 (_eprint: https://onlinelibrary.wiley.com/doi/pdf/10.1029/2009GL038607) doi: 10.1029/2009GL038607

Snoll, B., Ivanovic, R. F., Valdes, P. J., Maycock, A. C., & Gregoire, L. J. (2022, February). Effect of orographic gravity wave drag on Northern Hemisphere climate in transient simulations of the last deglaciation. *Climate Dynamics*. Retrieved 2022-03-01, from https://doi.org/10.1007/s00382-022-06196-2 doi: 10.1007/s00382-022-06196-2

Stanford, J. D., Rohling, E. J., Bacon, S., Roberts, A. P., Grousset, F. E., & Bolshaw, M. (2011, May). A new concept for the paleoceanographic evolution of Heinrich event 1 in the North Atlantic. *Quaternary Science Reviews*, *30*(9), 1047–1066. Retrieved 2020-02-28, from http://www.sciencedirect.com/science/article/pii/S0277379111000400 doi: 10.1016/j.quascirev.2011.02.003

Stern, J. V., & Lisiecki, L. E. (2013, July). North Atlantic circulation and reservoir age changes over the past 41,000 years. *Geophysical Research Letters*, *40*(14), 3693–3697. Retrieved 2020-03-13, from https://agupubs.onlinelibrary.wiley.com/doi/full/10.1002/grl.50679 doi: 10.1002/grl.50679

Stocker, T. F. (1998, October). The Seesaw Effect. *Science*, *282*(5386), 61–62. Retrieved 2021-11-11, from https://www.science.org/doi/full/10.1126/science.282.5386.61 (Publisher: American Association for the Advancement of Science) doi: 10.1126/science.282.5386.61

Stocker, T. F., & Johnsen, S. J. (2003). A minimum thermodynamic model for the bipolar seesaw. *Paleoceanography*, *18*(4). Retrieved 2021-11-11, from https://onlinelibrary.wiley.com/doi/abs/10.1029/2003PA000920 (_eprint: https://onlinelibrary.wiley.com/doi/pdf/10.1029/2003PA000920) doi: 10.1029/2003PA000920

Stockhecke, M., Timmermann, A., Kipfer, R., Haug, G. H., Kwiecien, O., Friedrich, T., ... Anselmetti, F. S. (2016, February). Millennial to orbital-scale variations of drought intensity in the Eastern Mediterranean. *Quaternary Science Reviews*, *133*, 77–95. Retrieved 2021-10-26, from https://www.sciencedirect.com/science/article/pii/S0277379115301979 doi: 10.1016/j.quascirev.2015.12.016

Stommel, H. (1961). Thermohaline Convection with Two Stable Regimes of Flow. *Tellus*, *13*(2), 224–230. Retrieved 2020-03-04, from https://onlinelibrary.wiley.com/doi/abs/10.1111/j.2153-3490.1961.tb00079.x (_eprint: https://onlinelibrary.wiley.com/doi/pdf/10.1111/j.2153-3490.1961.tb00079.x) doi: 10.1111/j.2153-3490.1961.tb00079.x

Tarasov, L., Dyke, A. S., Neal, R. M., & Peltier, W. R. (2012, January). A data-calibrated distribution of deglacial chronologies for the North American ice complex from glaciological modeling. *Earth and Planetary Science Letters*, *315-316*, 30–40. Retrieved 2020-03-08, from http://www.sciencedirect.com/science/article/pii/S0012821X11005243 doi: 10.1016/j.epsl.2011.09.010

Tarasov, L., & Peltier, R. W. (2002, July). Greenland glacial history and local geodynamic consequences. *Geophysical Journal International*, *150*(1), 198–229. Retrieved 2020-03-10, from https://academic.oup.com/gji/article/150/1/198/591943 (Publisher: Oxford Academic) doi: 10.1046/j.1365-246X.2002.01702.x

Thomas, E. R., Wolff, E. W., Mulvaney, R., Johnsen, S. J., Steffensen, J. P., & Arrowsmith, C. (2009). Anatomy of a Dansgaard-Oeschger warming transition: High-resolution analysis of the North Greenland Ice Core Project ice core. *Journal of Geophysical Research: Atmospheres*, *114*(D8). Retrieved 2021-01-28, from https://agupubs.onlinelibrary.wiley.com/doi/abs/10.1029/2008JD011215 (_eprint: https://agupubs.onlinelibrary.wiley.com/doi/pdf/10.1029/2008JD011215) doi: https://doi.org/10.1029/2008JD011215

Tierney, J. E., Zhu, J., King, J., Malevich, S. B., Hakim, G. J., & Poulsen, C. J. (2020, August). Glacial cooling and climate sensitivity revisited. *Nature*, *584*(7822), 569–573. Retrieved 2021-12-19, from https://www.nature.com/articles/s41586-020-2617-x doi: 10.1038/s41586-020-2617-x

Ullman, D. J., LeGrande, A. N., Carlson, A. E., Anslow, F. S., & Licciardi, J. M. (2014, March). Assessing the impact of Laurentide Ice Sheet topography on glacial climate. *Climate of the Past*, *10*(2), 487–507. Retrieved 2021-09-08, from https://cp.copernicus.org/articles/10/487/2014/ (Publisher: Copernicus GmbH) doi: 10.5194/cp-10-487-2014

Valdes, P. J., Armstrong, E., Badger, M. P. S., Bradshaw, C. D., Bragg, F., Davies-Barnard, T., ... Williams, J. H. T. (2017, October). The BRIDGE HadCM3 family of climate models: HadCM3@Bristol v1.0. *Geoscientific Model Development Discussions*. Retrieved 2020-07-09, from https://research-information.bris.ac.uk/en/publications/the-bridge-hadcm3-family-of-climate-models-hadcm3bristol-v10-2 (Publisher: Copernicus GmbH) doi: 10.5194/gmd-2017-16

Vettoretti, G., & Peltier, W. R. (2018, May). Fast Physics and Slow Physics in the Nonlinear Dansgaard–Oeschger Relaxation Oscillation. *Journal of Climate*, *31*(9), 3423–3449. Retrieved 2022-01-12, from https://journals.ametsoc.org/view/journals/clim/31/9/jcli-d-17-0559.1.xml (Important) doi: 10.1175/JCLI-D-17-0559.1

Vidal, L., Labeyrie, L., Cortijo, E., Arnold, M., Duplessy, J. C., Michel, E., ... van Weering, T. C. E. (1997, January). Evidence for changes in the North Atlantic Deep Water linked to meltwater surges during the Heinrich events. *Earth and Planetary Science Letters*, *146*(1), 13–27. Retrieved 2020-02-28, from http://www.sciencedirect.com/science/article/pii/S0012821X96001926 doi: 10.1016/S0012-821X(96)00192-6

Voelker, A. H. L. (2002, May). Global distribution of centennial-scale records for Marine Isotope Stage (MIS) 3: a database. *Quaternary Science Reviews*, *21*(10), 1185–1212. Retrieved 2020-03-04, from http://www.sciencedirect.com/science/article/pii/S0277379101001391 doi: 10.1016/S0277-3791(01)00139-1

Wang, X., Auler, A. S., Edwards, R. L., Cheng, H., Ito, E., Wang, Y., ... Solheid, M. (2007). Millennial-scale precipitation changes in southern Brazil over the past 90,000 years. *Geophysical Research Letters*, *34*(23). Retrieved 2021-10-26, from https://onlinelibrary.wiley.com/doi/abs/10.1029/2007GL031149 doi: 10.1029/2007GL031149

Wang, Y. J., Cheng, H., Edwards, R. L., An, Z. S., Wu, J. Y., Shen, C.-C., & Dorale, J. A. (2001, December). A High-Resolution Absolute-Dated Late Pleistocene Monsoon Record from Hulu Cave, China. *Science*, *294*(5550), 2345–2348. Retrieved 2021-10-21, from https://www.science.org/doi/10.1126/science.1064618 (Publisher: American Association for the Advancement of

Science) doi: 10.1126/science.1064618

Weber, M. E., Clark, P. U., Kuhn, G., Timmermann, A., Sprenk, D., Gladstone, R., ... Ohlwein, C. (2014, June). Millennial-scale variability in Antarctic ice-sheet discharge during the last deglaciation. *Nature*, *510*(7503), 134–138. Retrieved 2021-09-06, from https://www.nature.com/articles/nature13397 doi: 10.1038/nature13397

Wolff, E. W., Chappellaz, J., Blunier, T., Rasmussen, S. O., & Svensson, A. (2010, October). Millennial-scale variability during the last glacial: The ice core record. *Quaternary Science Reviews*, *29*(21), 2828–2838. Retrieved 2020-03-04, from http://www.sciencedirect.com/science/article/pii/S0277379109003588 doi: 10.1016/j.quascirev.2009.10.013

Zhang, X., Knorr, G., Lohmann, G., & Barker, S. (2017, July). Abrupt North Atlantic circulation changes in response to gradual CO_2 forcing in a glacial climate state. *Nature Geoscience*, *10*(7), 518–523. Retrieved 2019-10-02, from https://www.nature.com/articles/ngeo2974 doi: 10.1038/ngeo2974

Supporting Information for Millennial-scale climate oscillations triggered by deglacial meltwater discharge in last glacial maximum simulations

Yvan M. Romé[1], Ruza F. Ivanovic[1], Lauren J. Gregoire[1], Sam Sherriff-Tadano[1], Paul J. Valdes[2]

[1]School of Earth and Environment, University of Leeds, Leeds, UK

[2]School of Geographical Sciences, University of Bristol, Bristol, UK

Contents of this file

Introduction

The supporting information presented here contains eight sections and ten figures as supplements to the main text. This includes details on the last glacial maximum boundary conditions (section S1, Figure S1), the meltwater discharge protocol (section S2, figure S2), the global mean salinity correction algorithm (section S3), the smoothing bathymetry algorithm (section S4, Figures S3, S4, S5), the spectral analysis algorithm (section S5), the definition of warm and cold composite modes (section S6, Figures S6, S7, S8), the definition of the intertropical convergence zone index (section S7), the definition of the centre of mass (section S8), the definition of the average zones (Figures S9 and the mixed layer depth anomalies over the composite warm modes (Figures S10).

S1. Simulating the Last Glacial Maximum

For atmospheric trace gases, we adopted Last Glacial macimum (LGM) values of 190 ppm for CO_2 (Bereiter et al., 2015), 375 ppb for CH_4 (Loulergue et al., 2008), and a slightly lower concentration of 193 ppb for N_2O (compared to 200 ppb in the protocol) (Schilt et al., 2010), which corresponds to the 21 ka BP point in the interpolation between transient records of ice cores (Ivanovic et al., 2016). For the ice sheets, and associated fields, ice sheet extent, surface elevation and the resulting land-sea mask and ocean bathymetry were all derived from the GLAC-1D ice sheet reconstruction (Tarasov & Peltier, 2002; Tarasov et al., 2012; Briggs et al., 2014; Ivanovic et al., 2016) at year 21 ka BP. The ice sheet geometries (Figure S1) and associated palaeogeographical fields were not modified at any time of any simulations. The GLAC-1D reconstruction contains patches of ice over central Siberia and southern sectors of the Rocky Mountains (e.g. Tarasov et al., 2012) that can reach up to 100 m thick. Because they correspond to regions where the fractional ice mask is less than 0.5 (Ivanovic et al., 2016), these were not considered nor discussed further in this study.

The remaining parameters were set to the values indicated in Kageyama et al. (2017), including radiative forcing from insolation and dust.

S2. Meltwater discharge protocol

The algorithm used to create the meltwater discharge input was adapted from Ivanovic, Gregoire, Wickert, Valdes, and Burke (2017). At each 100-years time step and for each spatial grid cell where ice is present, ice elevation changes were converted into a freshwater-equivalent flux. To avoid generating strong peaks during the transformation of discrete snapshots of ice sheet geometry into a continuous time series, the flux was smoothed by taking the average of two consecutive time steps. Because we do not have a physically robust way to displace freshwater from the ocean back to the ice sheet, only ice losses were taken into account, ice accumulation being subsequently turned to zero. These steps can be summarised by equation S1, where $flux$ ($kg\, m^{-2}\, s^{-1}$) is the mass flux at a grid cell, $hice$ (m) the ice elevation at the same grid cell, $\rho = 1000\, kg\, m^{-3}$ water density, n represents the time step and $\Delta t = 100\, yrs$ the interval between two time steps.

$$flux_n = max(0, \rho \frac{hice_{n+1} - hice_n}{\Delta t}) \tag{S1}$$

Next, the 100-years time-step series was linearly interpolated into an annual series. The fluxes were then routed to an ocean cell following a global drainage network map consistent with GLAC-1D topography, using the routing coordinates provided with the PMIP4 last deglaciation protocol (Ivanovic et al., 2016). To be consistent with our model, this scattered discharge pattern was remapped to the coarser HadCM3 ocean grid, ensuring that the meltwater reaches the ocean by redistributing any routing points overlapping the land mask to their closest ocean cell.

Because the ocean model is a rigid-lid model (Gordon et al., 2000), oceanic freshwater forcing (including runoff, ice melting, precipitation/evaporation) is prescribed as virtual salinity fluxes. One possible consequence of this parameterisation is that large fluxes can lead to some grid cells being capped at 0 PSU (minimum salinity) in the case of large freshwater inputs. This can be problematic, since we would approach the limits of the equation of state (Bryan & Cox, 1972; Fofonoff & Millard Jr, 1983; Fofonoff, 1985), and would prevent the full freshwater forcing from being applied to the ocean during episodes of rapid, voluminous meltwater discharge. Instead of trying to estimate when the salinity saturation may be reached, we adopt a cautious approach by reproducing and updating the spreading algorithm employed by Ivanovic, Gregoire, Burke, et al. (2018) and Ivanovic, Gregoire, Wickert, and Burke (2018). This algorithm collects all the freshwater from its grid-cell point of entry to the ocean, and spreads it uniformly at the surface of neighbouring discharge regions of at least 500 m depth. The new version of the algorithm used here only modifies the definition of some spreading regions and collection boxes in accordance with the new inputs (i.e. the old algorithm would have missed some of the new meltwater fluxes as a new ice sheet and palaeogeography is being applied in accordance with GLAC-1D; the previous studies follow ICE-6G_C). These areas are plotted in Figure S2*b*. It is possible, although rare, that some discharge grid cells may not be caught by the spreading protocol. We checked at each time step that the residual's signal did not exceed 0.1% of the initial flux, a value we consider small enough to be thought of as noise.

Tests for a previous study (Ivanovic, Gregoire, Burke, et al., 2018) showed that there was a negligible difference between the results simulated using point-source or more distributed meltwater patterns during the Heinrich Stadial period, and although these freshwater fluxes are different (the previous study used the ICE-6G_C ice sheet history), they are of sufficiently similar rate/amplitude that we are confident that a similar inference applies to the new simulations presented here, whilst also ensuring that we avoid hitting the 0 PSU lower cap (see above).

The resulting fluxes, including the signal in key regions, are plotted in Figure S2*a*. Note the difference in this figure panel between smaller collection boxes (bold contours offshore), larger spreading regions (constituent coloured boxes), and key regions (colours) considered for plotting the fluxes (e.g. as time series in Figure S2*a*). Snapshots in time of the meltwater distribution are shown by Figure S2*c*.

Once the meltwater input file was created, we added the contribution of the river and iceberg run-off that was calculated to close the hydrological cycle during the Pre-Industrial. Note that meteoric runoff routing follows the configuration calculated when producing the HadCM3 PMIP4 LGM palaeogeography.

S3. Global mean salinity target

In multi-millennial simulations on the scale presented here, long-term drifts in global mean salinity can arise under equilibrium climate forcings due to internal imbalances in snowfall/melt and iceberg calving (which is prescribed and therefore cannot vary dynamically), and evaporation/precipitation over inland seas, which are not hydrologically connected to the ocean. To conserve water in the model and avoid these long-term drifts, we apply a method for keeping global mean salinity constant that distributes any required correction across the whole volume of the ocean. This approach was preferred to a surface correction, because the latter has a greater propensity for inducing surface salinity drifts that impact large scale ocean circulation, as concluded by Dentith, Ivanovic, Gregoire, Tindall, and Smith (2019). The method applied for this study is the VFLUX method described fully by Dentith et al. (2019). At each ocean model time step, global mean salinity is corrected so that the global mean salinity hits the prescribed target in accordance with the terrestrial ice volume and global ocean volume at that timestep with respect to the pre-industrial. The target is calculated following equation S2, where sal_{target} ($g\,kg^{-1}$) is the global salinity target of the experiment, $sal_{ref} = 34.83\,g\,kg^{-1}$ is the reference HadCM3 salinity at 0 ka, V_{ocn} (m^3) is the ocean volume at 0 ka BP and ΔV_{ice} (m^3) is the difference in ice volume between 0 ka BP and the current timestep of the simulation. Thus, even though the LGM ice sheet layout (i.e. as prescribed to the atmosphere model) stays constant in our experiments, the effects of changes in terrestrial ice volume on global mean ocean salinity are taken into account through the global salinity target. Thus, each simulation has a global mean salinity target that corresponds exactly with the ice sheet configuration at the time of the meltwater snapshot (Table 1), with the *CTRL* target set to $35.8334\,g\,kg^{-1}$.

$$sal_{target} = sal_{ref} * \frac{V_{ocn}}{V_{ocn} + \Delta V_{ice}} \tag{S2}$$

S4. Smoothing bathymetry algorithm

After a few thousand years of integration, five out of the seven simulations (*CTRL*, *21.5k*, *21k*, *19.4k*, *18.2k*) presented in this article crashed because of a stream function instability in the Philippines Sea. This instability takes the form of a dipole where two grid cells reach unsustainable high/low barotropic stream function values; for example, as shown for *CTRL* in Figure S3. A week (model time) before the crash, the instability is undetectable. When the pattern appears, it gets out of control in less than a simulated day. The precise cause of this crash is not known, but it always occurs at the same location and it appears to be related to the complex bathymetry of the region.

In order to tackle this issue, we restarted the runs having smoothed the bathymetry of the Philippines and South China Seas (Figure S4*f*). Because we cannot exactly determine the inception of the instability, we restarted the simulations a few model years/decades before the crashes: *CTRL* at year 2,800, *21.5k* at year 3,060, *21k* at year 2,650, *19.4k* at year 8,610 and *17.8k* at year 8,900. The same smoothing was applied to all simulations and all the other boundary conditions remain unchanged. After this one intervention, all experiments successfully ran to completion.

Small disruptions of the climate are induced by the smoothing and restart process. For example, there is a slight increase of long-term drifts in *CTRL* (Figure S5), probably caused by a slight perturbation to the equilibrium state from introducing a small amount of noise at the restart alongside the smoothing of South China Sea and Indonesian bathymetry; the model is adjusting to the minor modifications. However, the trends are of the same order of magnitude as in the previous two and a half thousand years of simulation, and significantly smaller than during the last one thousand years of spin-up, implying that climate remains close to its equilibrium state. Similar changes in the long term drifts are seen in *21.5k* and *21k* (not shown), but are impossible to assess for *19.4k* and *17.8k* because of their oscillatory variability. Nonetheless, any impact of the smoothing and restart on the oscillations is imperceptible if it is exists at all. After the introduction of the smoothed dumps (arrows in Figure 3*b*), there is no significant change of behaviour in any of the time series. We cannot determine conclusively whether the smoothing influences the periodicity of the oscillations. However, the climate and ocean behaviours at the end of the restarted simulations are consistent with the variability observed before the smoothing.

Here, we show the spatial response induced by the change of bathymetry for *CTRL* only (Figure S4), but all the other simulations were analysed and returned comparable results. The resulting smoothed bathymetry has the greatest impact on the surface air temperatures, sea surface temperatures and sea surface salinity in the Philippines Sea and the Sea of Japan, with changes of up to 7°C, 8°C and 5 $g\,kg^{-1}$ respectively, but only in grid cells very local to the bathymetric modifications. Outside of these cells, the effect is either very small or statistically insignificant. In particular, we do not see any significant response from the climate system in the North Atlantic, which is the primary domain of interest for this study. In conclusion, we infer that the modifications induced by smoothing South China Sea and Indonesian bathymetry mid-run are minor and do not impact the main findings of the study.

S5. Spectral analysis of the oscillating simulations

Averaging model outputs over time, whether it is by using running means or taking snapshots, is a useful tool for assessing the main trends of a simulation. The downside is that we lose information on the dynamics and variability that are shorter/faster or of comparable duration to the length of the averaging period. Because our aim is to focus on millennial-scale variability only, we here propose a method based on spectral analysis.

Fourier theory, implemented in the Scilab Python project, allows for calculating the harmonics and the Power Spectral Density (PSD) of a time series. By applying that method to the simulated time series of Greenland temperatures at the NGRIP site, we derive a spectrum for each *oscillating* and *slow-recovery* simulations in $4c$. Note that the mean value of the signals were subtracted before calculating the PSD to compensate the offset from the fixed component (at 0 Hz). The amplitude of the harmonics corresponds to the most significant frequencies in the time series' signals. The frequencies of millennial-scale variability peak around $10^{-3}\,yrs^{-1}$ (corresponding to a period of $1000\,yrs$), while the frequencies associated with inter-annual variability are higher around $1\,yrs^{-1}$. In *oscillating simulations*, we do indeed observe a clear dominant periodicity of about a thousand years, which corresponds to frequencies previously estimated from Figure 3. On the other hand, *18.2k* does not display such a significant peak in the Fourier space and cannot, therefore, be considered as quasi-oscillating. In order to only conserve millennial-scale events and filter inter-annual signal, we decided to apply a first-order low pass filter calibrated with a cut-off frequency of $2 \times 10^{-3}\,yrs^{-1}$ (corresponding to a period of $5000\,yrs$). This is slightly higher than the dominant frequency of the *oscillating simulations* in order not to lose the information contained in the smaller secondary peaks, mainly observed in *17.8k*. This cut-off frequency, and consequently the filters, are the same for every simulation. The resulting filtered signals are shown by Figure 4*b*.

Compared to the NGRIP temperatures running mean series of Figure 3*c*, Figure 4*b* provides a clearer view of the main features of our time series and neither the periodicity of the signals nor the range of temperatures are significantly altered. Nonetheless, we still note a smoothing during sharper climate changes, where some information contained in higher frequencies may have been obscured by the processing. For example, we do not observe the overshoots at the onset of some warm phases in the filtered signals, and the most extreme warming/cooling rates are also damped.

This spectral analysis is useful for quantitatively assessing *oscillating simulations* with dominant frequencies around a thousand years, but fall short of providing useful information for lower dominant frequencies. For instance, the algorithm does not capture the longer periodicity (of a few thousand years) of *18.2k*. This is because Fourier transforms require a sufficient number of cycles to compute robustly. Hence, our algorithm does not have enough material to establish either way whether the *18.2k* simulation is slowly oscillating, or showing other behaviour such as a complex permanent recovery. Similarly, but more extreme, the absence of a periodic signal in the *warm simulations* prevents the Fourier analysis from being correctly handled, and their responses were therefore not included in this analysis.

For all the stated reasons, we emphasise that it is not appropriate to use the frequency analysis alone to understand our simulations. Instead, we utilise such an approach to complement the running-mean analysis, contributing an objective quantification of cyclical behaviour to identify oscillations, determine the main frequencies of the millennial-scale variability, and isolate the typical features within our experiments. It also helps to clarify the dynamics of the simulations, which is useful for understanding the behaviours depicted by Figure 6.

S6. Definition of warm and cold composite modes

In order to accurately characterise the simulations in this study, it is useful to be able to analyse aggregate features of the cold and warm climate modes, e.g. as presented in Figures 5. The intricate climate response of the meltwater simulations makes it difficult to adopt an objective definition that is commonly applicable to all simulations of cold and warm modes. A simple approach could be to define a fixed period of time before, after or spanning either side of the coldest/warmest points of the time series. However, this relatively unintelligent algorithm would be heavily susceptible to biases. For example, the warm modes could be biased towards the overshoot during the recovery phase, and the cold modes by the initial transition to a weak AMOC stage. Trying to widen the time spans to avoid this would result in the inclusion of the transition times. A further consideration is that the results need to be consistent between the NGRIP temperatures and the AMOC index time series despite the small lag between the two.

In light of these remarks, six different methods were tested to design the optimal algorithm for identifying the composite data for the cold and warm modes in our simulations, as depicted in Figures S6 and S7. *Method 1* defines the warm and cold modes as the highest and lowest thirds of the 30-year running mean AMOC index time series. *Method 1b* is similar, only it defines the warm and cold modes on the *filtered* time series of the AMOC index. *Method 2* defines the warm and cold modes as the highest and lowest thirds of the 30-year running mean NGRIP temperature time series. *Method 3* defines the warm and cold modes as the highest and lowest quarters of the 30-year running mean AMOC index time series, excluding the first 1000 years for all experiments except *21.5k* and *21k* to define the quarters; *20.7k*, *19.4k*, *18.2k* and *17.8k* generally show better consistency after the first 1000 years, excluding their adjustment to the initial meltwater perturbation, which has a strong early impact in these simulations. In *Method 4*, we manually defined the warm and cold limits for each simulation to visually fit what looks like a warm or cold period from the 30-year running mean AMOC index time series. *Method 5* defines the warm modes as the 150 year period centred around the maximum of the filtered AMOC time series and the cold modes as the 150 year period centred around the minimum of the AMOC time series. The maximum and minimum have to be spaced 500 years apart and in the highest/lowest thirds and concave/convex for warm/cold modes.

Comparing the effects of each algorithm on the zonal mean anomalies in Figure S8, we observe consistent behaviours during cold modes and slightly more variability in warm modes despite showing similar zonal mean patterns. *Method 3* returns a stronger AMOC in both cold and warm modes of the oscillating and slow-recovery simulations, with the lowest sea ice cover in warm modes. *Method 2* also tends to simulate warmer weak modes of the oscillating and warm experiments. *Method 1* and *Method 5*'s definition of warm modes is too broad in the warm simulations, leading to 1°C cooling of the warm modes. A significant amount of the transition times in cold modes are included in *Method 1* and *Method 3*. Finally, we do not recommend using the filtered time series for non-oscillating simulations as they create artefacts in the NGRIP time series that affect the modes-selection algorithm, which rules out methods Method 1b and *Method 5* from being useful.

Method 4 is the only approach not to present any strong irregularities in the composite warm/cold modes. Although it relies on a visual identification, which could induce bias, the results always rank within the mean behaviour in zonal mean anomalies. The method is simple, but provides the required information needed for the analysis. It is the algorithm that best filters-out the transition periods between the cold and warm phases, and it has the advantage of being easily adaptable and applied to all six simulations. It is, therefore, the algorithm we adopted for this study.

We note that when the amplitude range is small compared to the running mean variability, such as in *21.5k*, some time slices may end up being assigned to the wrong mode by the chosen categorisation method (*Method 4*). Nonetheless, this is infrequent and easy enough to identify (e.g. in Figures 5g and 5n); thus we can identify that it does not have a significant impact on the presented results.

S7. Intertropical Convergence Zone (ITCZ) index

The Intertropical Convergence Zone (ITCZ) index (Figure 3) was inspired by the work of (Braconnot et al., 2007) and Singarayer, Valdes, and Roberts (2017) and corresponds to the mean northern limit of the ITCZ. It was calculated following equation S3, where $lat(pr_{max})$ is the latitude of the maximum zonally averaged precipitation, pr $(kg\,m^{-2}\,s^{-1})$. Compared to Singarayer et al. (2017), we computed the mean latitude instead of the maximum latitude of the rainbelt to gain a better view of the global displacement of the ITCZ.

$$ITCZ_{index} = mean(\frac{\sum_{y=lat(pr_{max})}^{35^\circ N} pr(lon, y) lat(y)}{\sum_{y=lat(pr_{max})}^{35^\circ N} lat(y)}) \tag{S3}$$

S8. Locating the centre of mass

The lontitude and latitude of the centre of mass of a value $V(lon, lat)$ (used in section 6 and Figure 6) is defined in equation S4. For the sake of simplicity, the volume of each grid cell was not considered in this definition.

$$[lon_{COM}, lat_{COM}]_V = \frac{\sum_{i,j} V(i,j)[lon(i), lat(j)]}{\sum_{i,j} V(i,j)} \tag{S4}$$

C1. Caption for figure S2

a. Meltwater discharge history over the early deglaciation and its distribution over the main regions defined in panel *b*. This plot incorporates the 200-years smoothing described in section S2). Vertical bars represent the time steps chosen for calculating each constant meltwater-forcing snapshot (see section 2.2, and Table 1). *b.* Map of ice meltwater collection and spreading areas. Each individual box corresponds to a freshwater collection area, redistributed to the corresponding spreading areas (within the same box) indicated by the bold contours. Seven main regions were defined for the presented analysis, as labelled on the right (colours). Note that these regions do not correspond to individual regions but rather to clusters of spreading areas. The colour coding matches panel *a*. *c.* Ice sheet meltwater discharge snapshot used for each perturbed meltwater simulation. The names and colours of the simulations correspond to the snapshot time on panel *b*. The colour coding of each simulation matches figures in the main text. Please note the logarithmic scale.

C2. Caption for figure S6

Depiction of the constituent data (here, showing the AMOC index; max Atlantic overturning circulation at 26.5° N) for the warm and cold climate phases arising from the different methods for creating the composite warm and cold modes analysed in the main article (introduced in section 4). Panels *a*, *c*, *d* and *e* used 30-year running-mean of the AMOC index time series. Panels *b* and *f* used the filtered AMOC index time series as described in section S5. See Section S6 text for the detail of the different methods.

C3. Caption for figure S7

Depiction of the constituent data (here, showing the NGRIP surface air temperature, 42.32° W, 75.01° N) for the warm and cold climate phases arising from the different methods for creating the composite warm and cold modes analysed in the main article (introduced in section 4). Panels *a*, *c*, *d* and *e* show the 30-year running-mean of the NGRIP temperature time series. Panels *b* and *f* show the filtered NGRIP temperature time series as described in section S5. See S6 text for the detail of the different methods.

C4. Caption for figure S8

Composite warm and cold modes mean zonal anomalies between the meltwater simulations and the reference state in the Atlantic (70° W – 10° E). Solid lines are cold modes and dashed lines are warm modes, which have been compiled using the five methods described in the text (section S6). Panels show the zonally averaged surface air temperature, sea surface temperature, mixed layer depth, winter sea ice concentration, summer sea ice and maximum overturning circulation flow over the water column for the different methods and applied to three simulations corresponding to the three different clusters identified in section 4. Figures S6 and S7 highlight the constituent data for the warm and cold modes identified by each method.

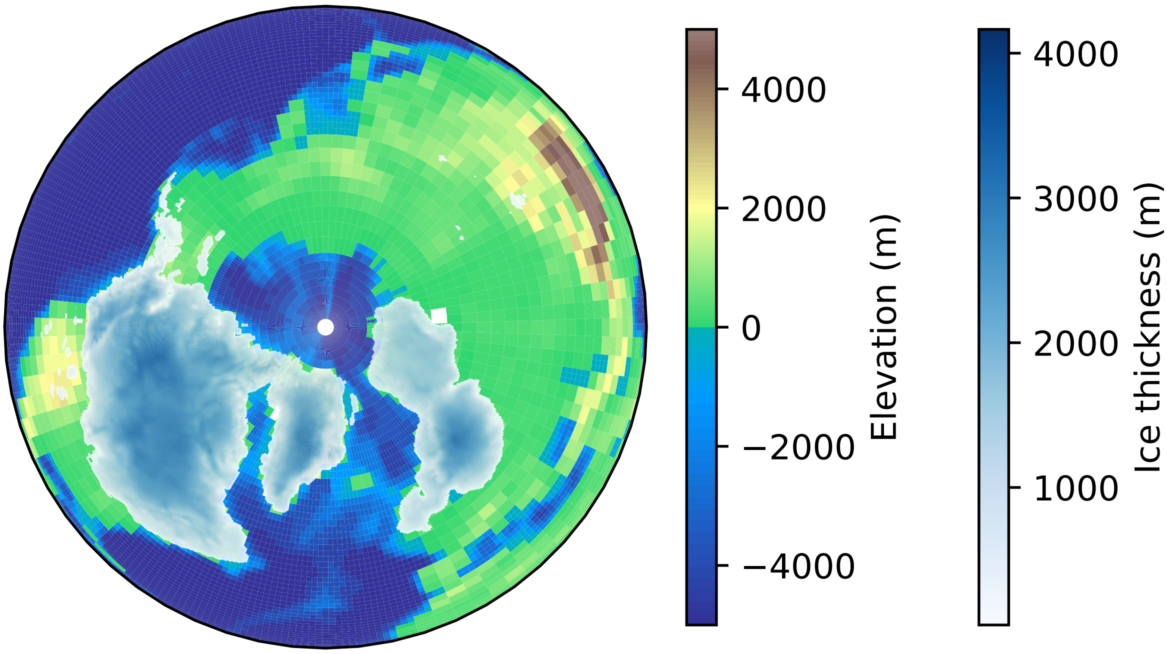

Figure S1. Orography, bathymetry, land sea mask and ice sheet elevation boundary conditions in the Arctic region. Ice sheets were reconstructed from GLAC-1D at 21 ka BP. Terrestrial ice is shown where it is thicker than 50 m.

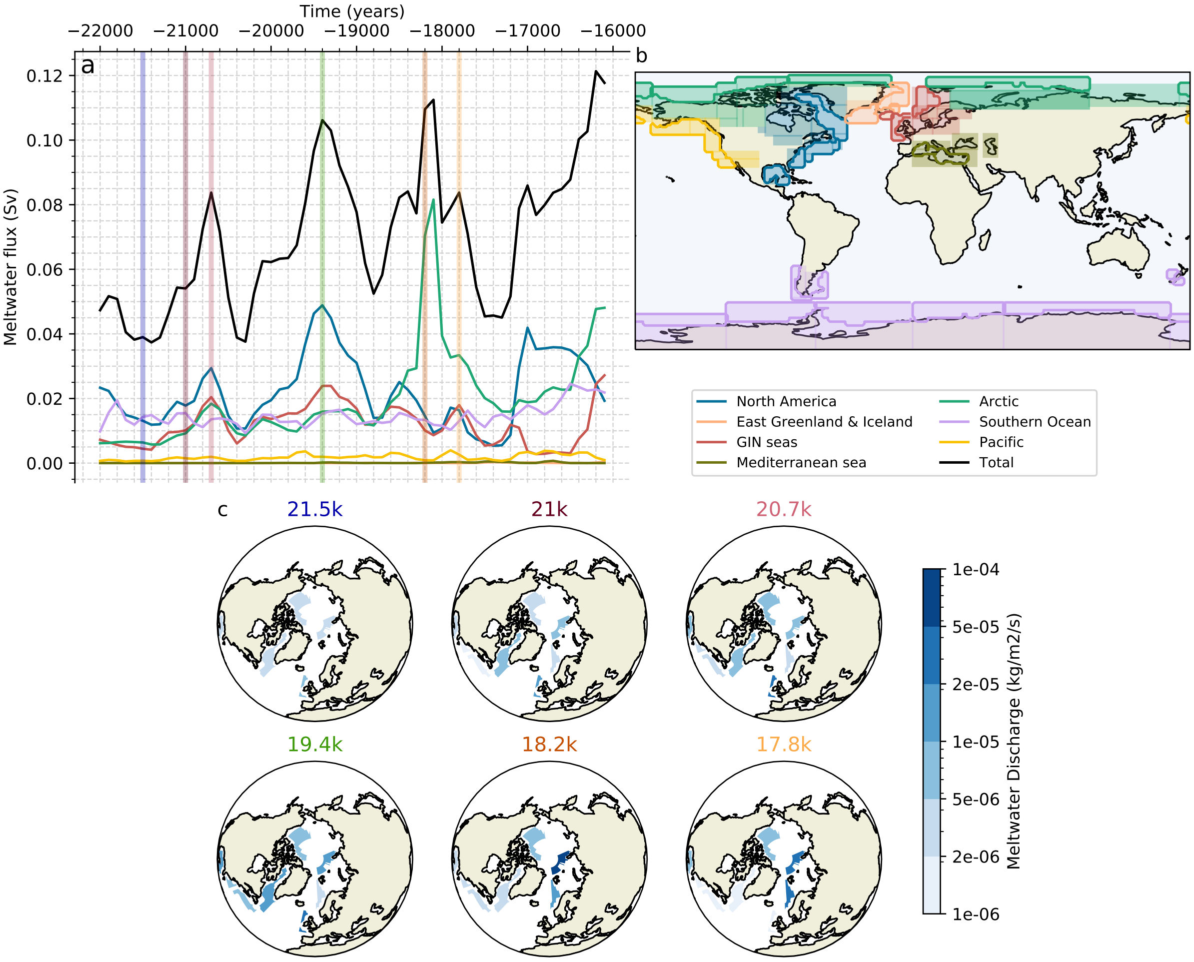

Figure S2. See Caption C1.

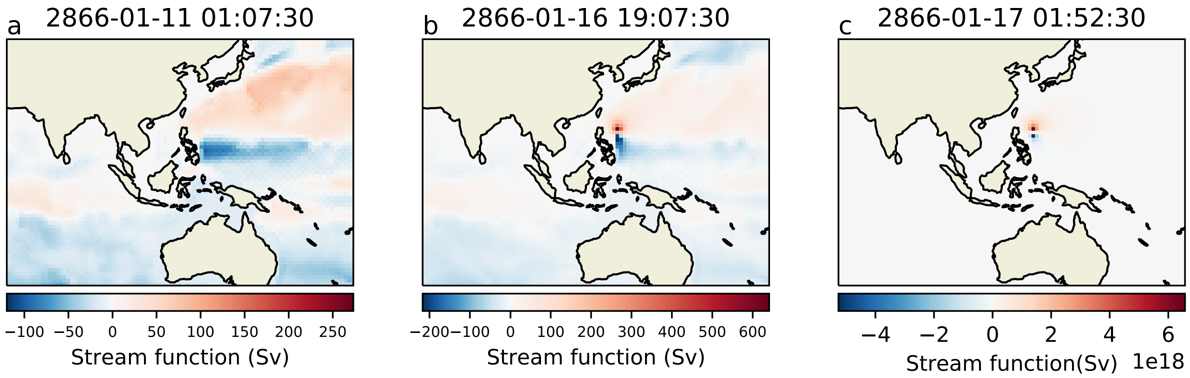

Figure S3. *a.* Barotropic stream function in *CTRL* during the simulated week before numerical instability causes the model to crash, *b.* at the development of the instability and *c.* at the time of the crash. Note the difference in scales.

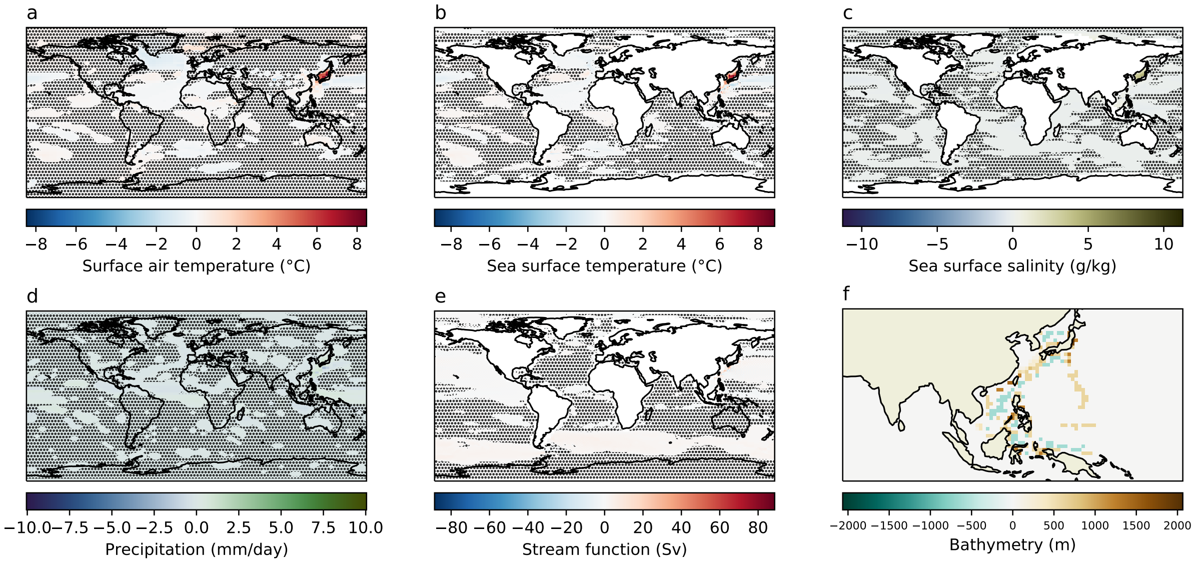

Figure S4. *a.*Changes in surface air temperature, *b.* sea surface temperature, *c.* surface salinity, *d.* precipitation, *e.* stream function and *f.* bathymetry in *CTRL* after applying the smoothing algorithm (using the pre/post-smoothing time windows defined in Figure S5). Hatching is applied where values are considered statistically insignificant using a student t-test with a p-value of 0.1 .

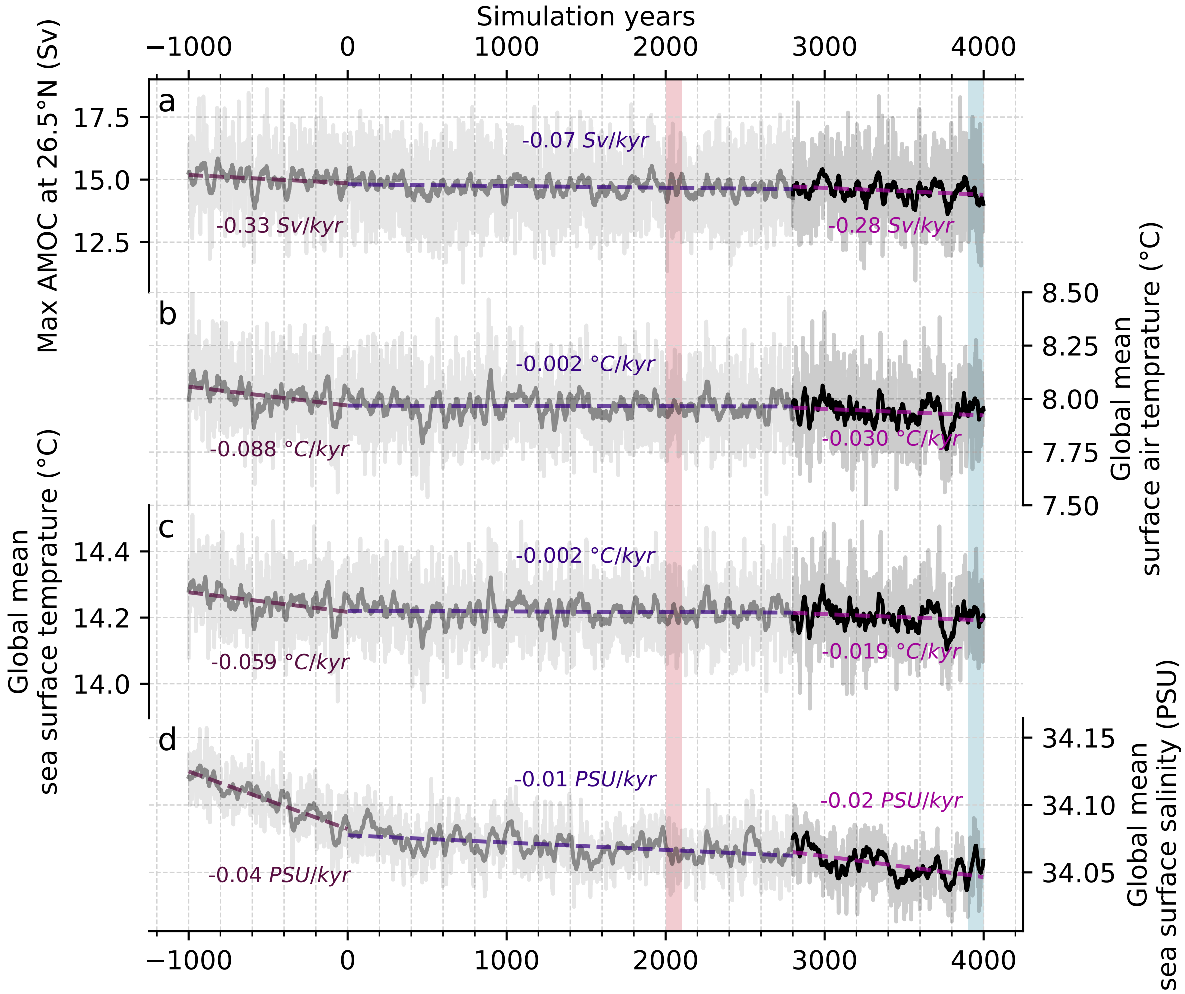

Figure S5. *a.* AMOC index, *b.* global mean surface air temperature, *c.* sea surface temperature and *d.* sea surface salinity trends in the *CTRL* simulation. Light/dark colours correspond to before/after the application of the smoothing algorithm, respectively. The last thousand years of spin-up are shown at the start of the run, for context. The drifts (purple) are calculated from linear regression of the time series before (darker purple) and after (lighter purple) the restart of the run and during the last thousand years of spin-up (medium purple). Red and blue shading highlights the pre and post smoothing phases used in Figure S4, respectively

.

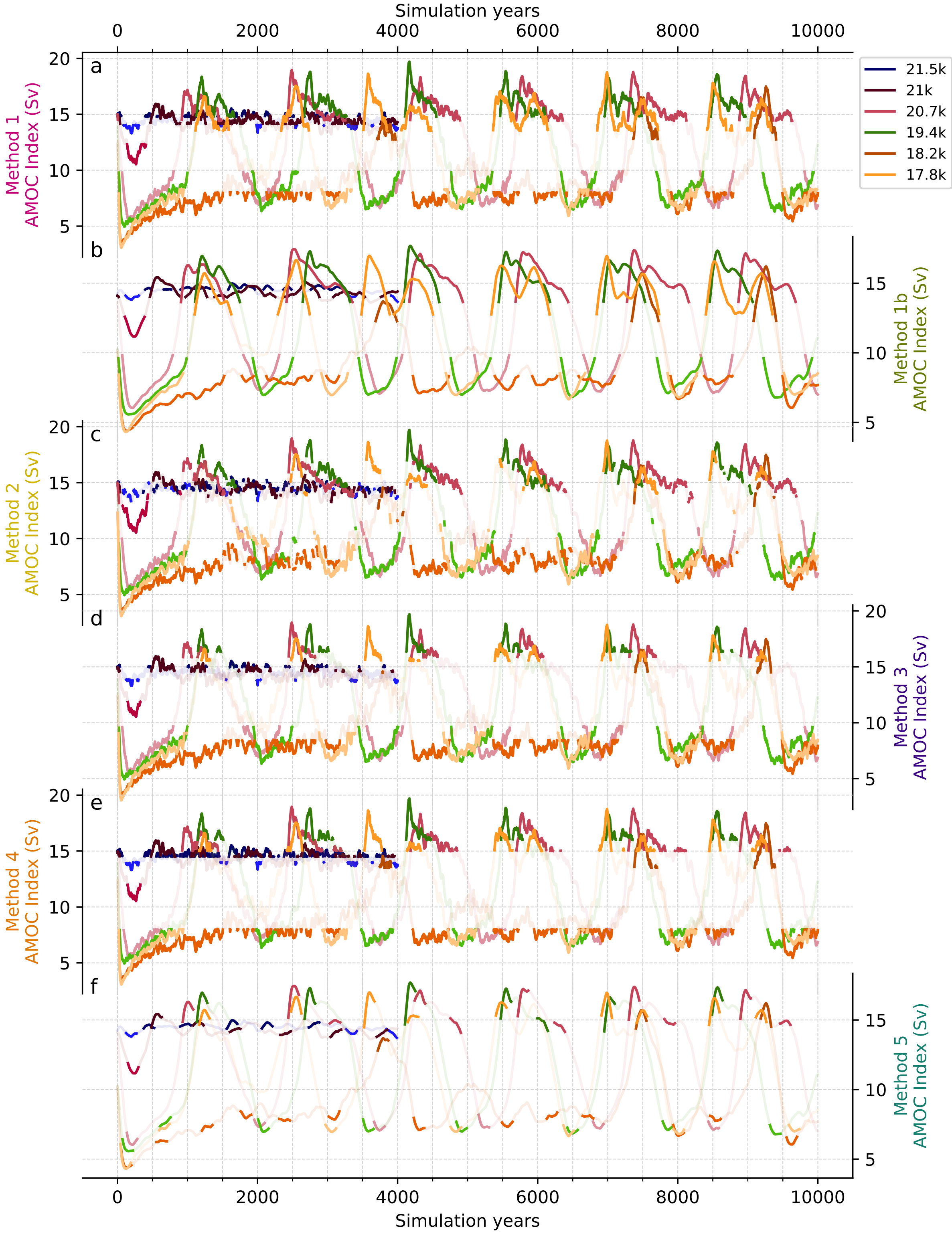

Figure S6. See Caption C2.

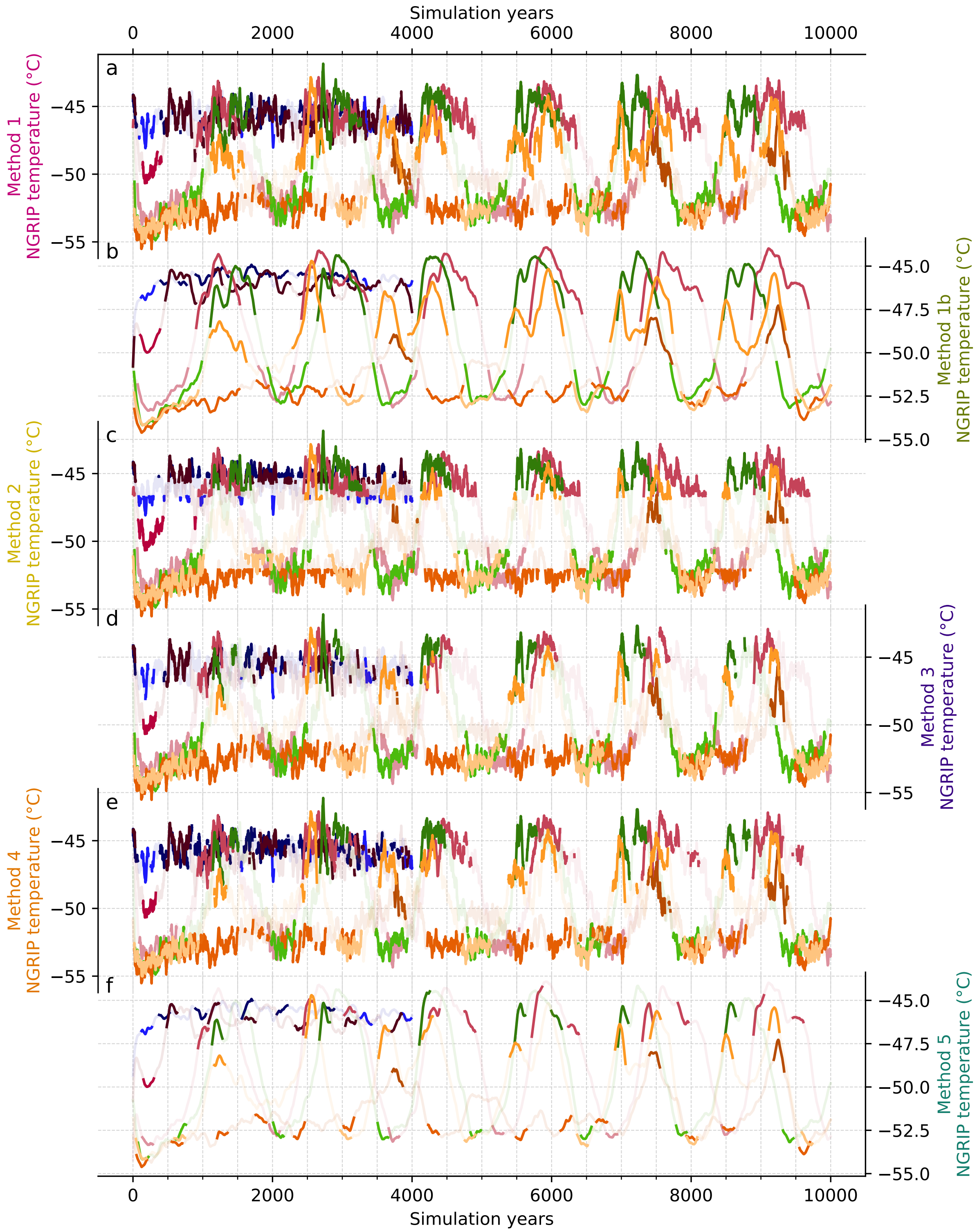

Figure S7. See Caption C3.

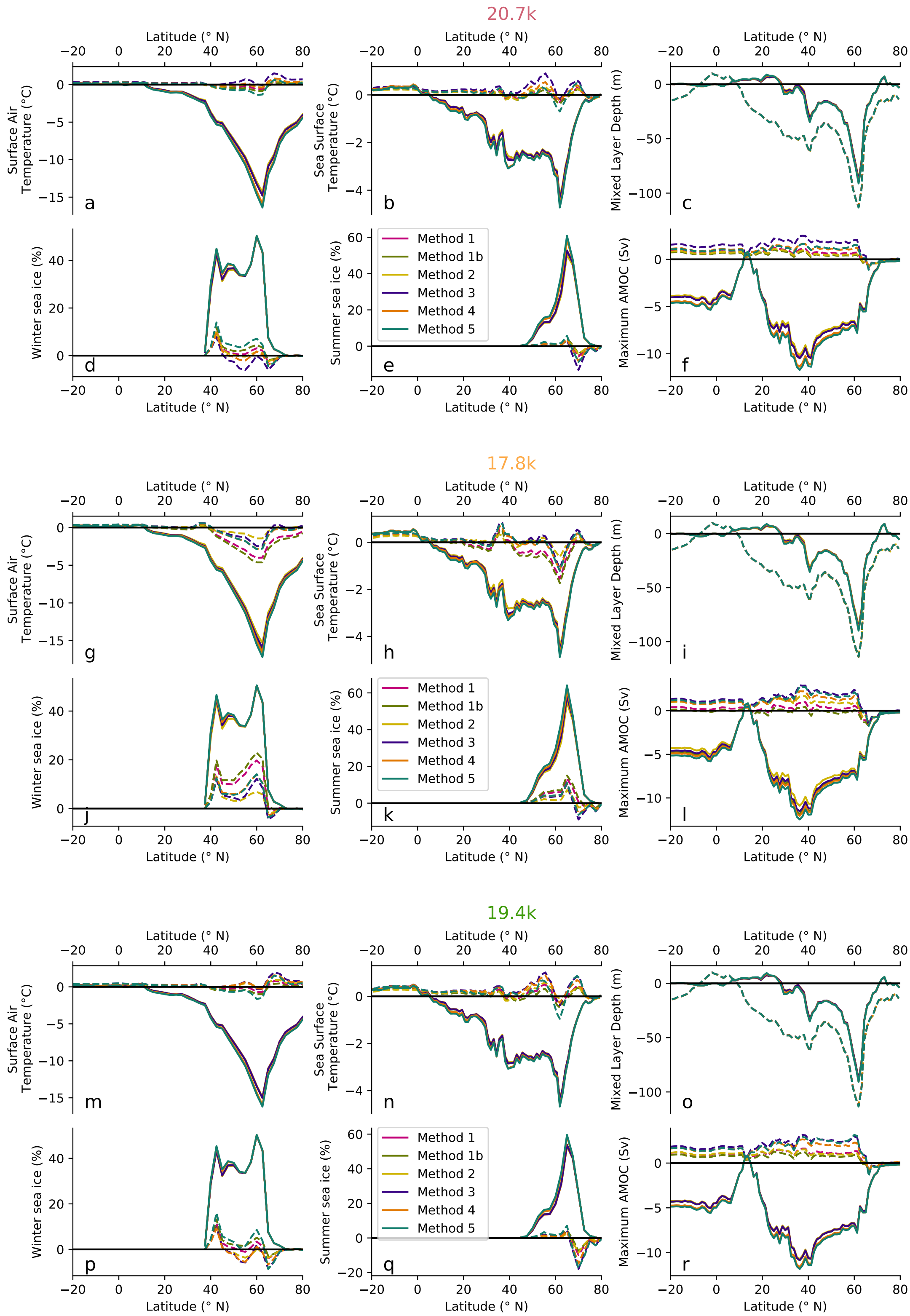

Figure S8. See Caption C4.

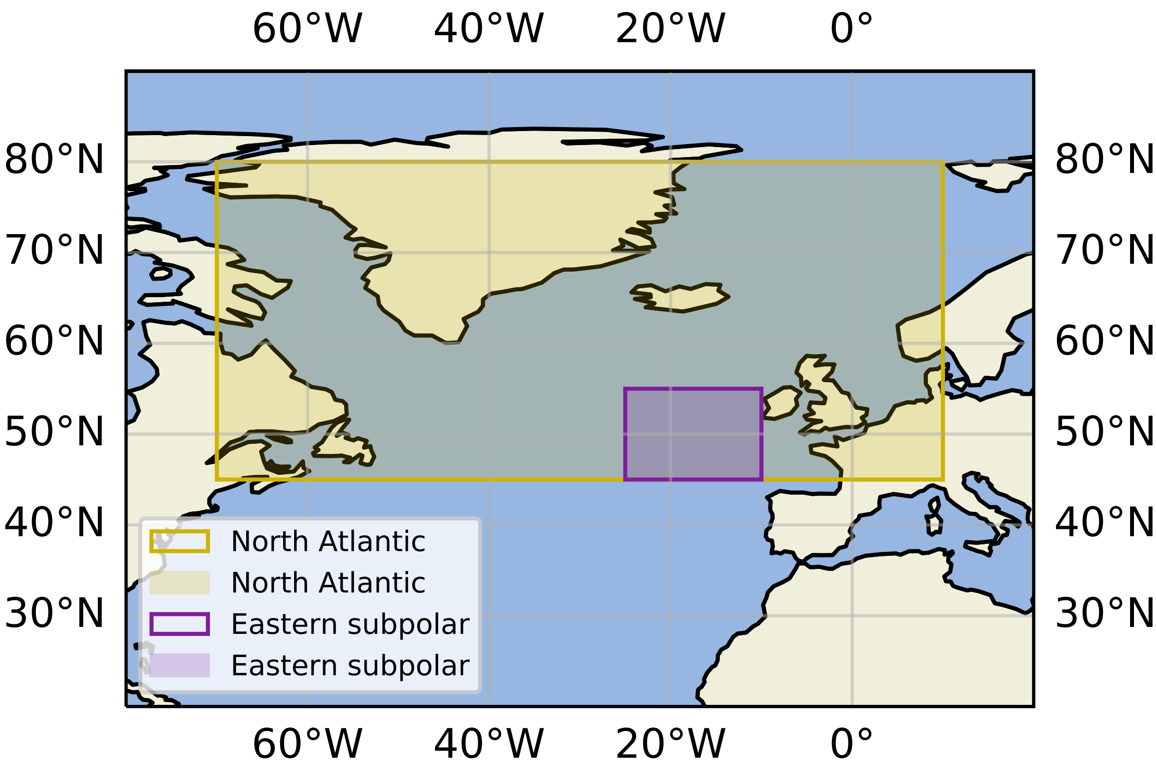

Figure S9. Definition of North Atlantic zones used for the analysis summarised by Figure 6.

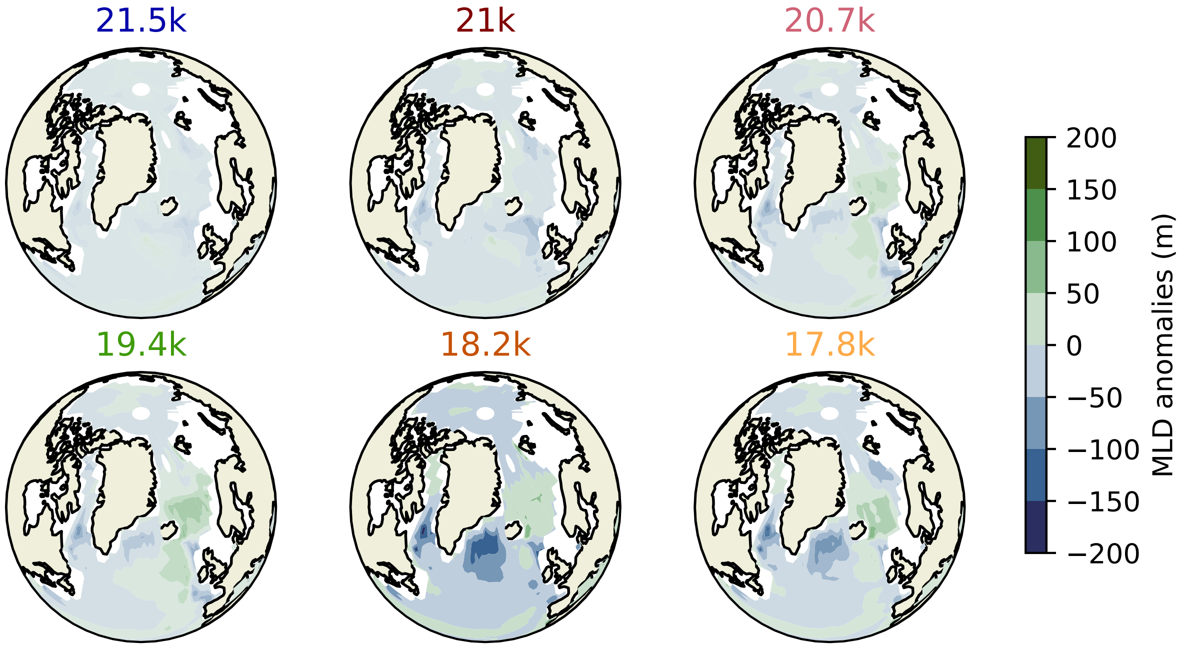

Figure S10. Mean annual mixed layer depth anomalies between the meltwater simulations and *CTRL* over the composite warm modes.

References

Bereiter, B., Eggleston, S., Schmitt, J., Nehrbass-Ahles, C., Stocker, T. F., Fischer, H., ... Chappellaz, J. (2015). Revision of the EPICA Dome C CO2 record from 800 to 600 kyr before present. *Geophysical Research Letters*, *42*(2), 542–549. Retrieved 2020-03-10, from `https://agupubs.onlinelibrary.wiley.com/doi/abs/10.1002/2014GL061957` (_eprint: https://agupubs.onlinelibrary.wiley.com/doi/pdf/10.1002/2014GL061957) doi: 10.1002/2014GL061957

Braconnot, P., Otto-Bliesner, B., Harrison, S., Joussaume, S., Peterchmitt, J.-Y., Abe-Ouchi, A., ... Zhao, Y. (2007, June). Results of PMIP2 coupled simulations of the Mid-Holocene and Last Glacial Maximum – Part 2: feedbacks with emphasis on the location of the ITCZ and mid- and high latitudes heat budget. *Climate of the Past*, *3*(2), 279–296. Retrieved 2022-02-02, from `https://cp.copernicus.org/articles/3/279/2007/` (Publisher: Copernicus GmbH) doi: 10.5194/cp-3-279-2007

Briggs, R. D., Pollard, D., & Tarasov, L. (2014, November). A data-constrained large ensemble analysis of Antarctic evolution since the Eemian. *Quaternary Science Reviews*, *103*, 91–115. Retrieved 2020-03-08, from `http://www.sciencedirect.com/science/article/pii/S0277379114003448` doi: 10.1016/j.quascirev.2014.09.003

Bryan, K., & Cox, M. D. (1972, October). An Approximate Equation of State for Numerical Models of Ocean Circulation. *Journal of Physical Oceanography*, *2*(4), 510–514. Retrieved 2021-09-07, from `https://journals.ametsoc.org/view/journals/phoc/2/4/1520-0485_1972_002_0510_aaeosf_2_0_co_2.xml` doi: 10.1175/1520-0485(1972)002⟨0510:AAEOSF⟩2.0.CO;2

Dentith, J. E., Ivanovic, R. F., Gregoire, L. J., Tindall, J. C., & Smith, R. S. (2019, February). Ocean circulation drifts in multi-millennial climate simulations: the role of salinity corrections and climate feedbacks. *Climate Dynamics*, *52*(3), 1761–1781. Retrieved 2021-10-28, from https://doi.org/10.1007/s00382-018-4243-y doi: 10.1007/s00382-018-4243-y

Fofonoff, N. P. (1985). Physical properties of seawater: A new salinity scale and equation of state for seawater. *Journal of Geophysical Research: Oceans*, *90*(C2), 3332–3342. Retrieved 2021-09-07, from https://agupubs.onlinelibrary.wiley.com/doi/abs/10.1029/JC090iC02p03332 doi: 10.1029/JC090iC02p03332

Fofonoff, N. P., & Millard Jr, R. C. (1983). Algorithms for the computation of fundamental properties of seawater. *UNESCO Technical Papers in Marine Sciences*. Retrieved 2021-09-07, from https://repository.oceanbestpractices.org/handle/11329/109 doi: 10.25607/OBP-1450

Gordon, C., Cooper, C., Senior, C. A., Banks, H., Gregory, J. M., Johns, T. C., ... Wood, R. A. (2000, February). The simulation of SST, sea ice extents and ocean heat transports in a version of the Hadley Centre coupled model without flux adjustments. *Climate Dynamics*, *16*(2), 147–168. Retrieved 2020-07-09, from https://doi.org/10.1007/s003820050010 doi: 10.1007/s003820050010

Ivanovic, R. F., Gregoire, L. J., Burke, A., Wickert, A. D., Valdes, P. J., Ng, H. C., ... Dentith, J. E. (2018). Acceleration of Northern Ice Sheet Melt Induces AMOC Slowdown and Northern Cooling in Simulations of the Early Last Deglaciation. *Paleoceanography and Paleoclimatology*, *33*(7), 807–824. Retrieved 2019-10-02, from https://agupubs.onlinelibrary.wiley.com/doi/abs/10.1029/2017PA003308 doi: 10.1029/2017PA003308

Ivanovic, R. F., Gregoire, L. J., Kageyama, M., Roche, D. M., Valdes, P. J., Burke, A., ... Tarasov, L. (2016, July). Transient climate simulations of the deglaciation 21–9 thousand years before present (version 1) – PMIP4 Core experiment design and boundary conditions. *Geoscientific Model Development*, *9*(7), 2563–2587. Retrieved 2020-02-20, from https://www.geosci-model-dev.net/9/2563/2016/ doi: https://doi.org/10.5194/gmd-9-2563-2016

Ivanovic, R. F., Gregoire, L. J., Wickert, A. D., & Burke, A. (2018). Climatic Effect of Antarctic Meltwater Overwhelmed by Concurrent Northern Hemispheric Melt. *Geophysical Research Letters*, *45*(11), 5681–5689. Retrieved 2021-04-05, from https://agupubs.onlinelibrary.wiley.com/doi/abs/10.1029/2018GL077623 (_eprint: https://agupubs.onlinelibrary.wiley.com/doi/pdf/10.1029/2018GL077623) doi: https://doi.org/10.1029/2018GL077623

Ivanovic, R. F., Gregoire, L. J., Wickert, A. D., Valdes, P. J., & Burke, A. (2017). Collapse of the North American ice saddle 14,500 years ago caused widespread cooling and reduced ocean overturning circulation. *Geophysical Research Letters*, *44*(1), 383–392. Retrieved 2020-07-09, from https://agupubs.onlinelibrary.wiley.com/doi/abs/10.1002/2016GL071849 (_eprint: https://agupubs.onlinelibrary.wiley.com/doi/pdf/10.1002/2016GL071849) doi: 10.1002/2016GL071849

Kageyama, M., Albani, S., Braconnot, P., Harrison, S. P., Hopcroft, P. O., Ivanovic, R. F., ... Zheng, W. (2017, November). The PMIP4 contribution to CMIP6 – Part 4: Scientific objectives and experimental design of the PMIP4-CMIP6 Last Glacial Maximum experiments and PMIP4 sensitivity experiments. *Geoscientific Model Development*, *10*(11), 4035–4055.

Retrieved 2020-02-20, from https://www.geosci-model-dev.net/10/4035/2017/ doi: https://doi.org/10.5194/gmd-10-4035-2017

Loulergue, L., Schilt, A., Spahni, R., Masson-Delmotte, V., Blunier, T., Lemieux, B., ... Chappellaz, J. (2008, May). Orbital and millennial-scale features of atmospheric CH 4 over the past 800,000 years. *Nature*, *453*(7193), 383–386. Retrieved 2020-03-10, from https://www.nature.com/articles/nature06950 (Number: 7193 Publisher: Nature Publishing Group) doi: 10.1038/nature06950

Schilt, A., Baumgartner, M., Schwander, J., Buiron, D., Capron, E., Chappellaz, J., ... Stocker, T. F. (2010, November). Atmospheric nitrous oxide during the last 140,000years. *Earth and Planetary Science Letters*, *300*(1), 33–43. Retrieved 2020-03-10, from http://www.sciencedirect.com/science/article/pii/S0012821X10006023 doi: 10.1016/j.epsl.2010.09.027

Singarayer, J. S., Valdes, P. J., & Roberts, W. H. G. (2017, August). Ocean dominated expansion and contraction of the late Quaternary tropical rainbelt. *Scientific Reports*, *7*(1), 9382. Retrieved 2022-01-21, from https://www.nature.com/articles/s41598-017-09816-8 doi: 10.1038/s41598-017-09816-8

Tarasov, L., Dyke, A. S., Neal, R. M., & Peltier, W. R. (2012, January). A data-calibrated distribution of deglacial chronologies for the North American ice complex from glaciological modeling. *Earth and Planetary Science Letters*, *315-316*, 30–40. Retrieved 2020-03-08, from http://www.sciencedirect.com/science/article/pii/S0012821X11005243 doi: 10.1016/j.epsl.2011.09.010

Tarasov, L., & Peltier, R. W. (2002, July). Greenland glacial history and local geodynamic consequences. *Geophysical Journal International*, *150*(1), 198–229. Retrieved 2020-03-10, from https://academic.oup.com/gji/article/150/1/198/591943 (Publisher: Oxford Academic) doi: 10.1046/j.1365-246X.2002.01702.x